https://doi.org/10.5194/essd-2026-324
Preprint. Discussion started: 12 May 2026

Open Access Earth System Science Data Discussions

The Southern Andes Daily Snow Depth Dataset (2010–2024): Quality–Controlled Dataset from Chile and Argentina

Alexis Caro[1], Javier Medina[2,3], Freddy Saavedra[2,3,4], Fernando Gimeno[5,6], Jorge Huenante[7], Mariano Masiokas[8], Cristian Orrego[9], Ana Hernández[2,3,4], James McPhee[10,11], Pierre Pitte[8], Sebastián Krogh[12], David Farias–Barahona[1], Nevenka Bulovic[13], Iñigo Irarrazaval[14], Shelley MacDonell[9,15], Mauricio Zambrano-Bigiarini[6,16], Carlos Romero[2,3,4]

[1]Department of Geography, Universidad de Concepción, Concepción, Chile
[2]Laboratorio de Teledetección Ambiental, Universidad de Playa Ancha, Valparaíso, Chile
[3]HUB Ambiental, Universidad de Playa Ancha, Valparaíso, Chile
[4]Universidad de Playa Ancha, Valparaíso, Chile
[5]Doctorado en Ciencias de Recursos Naturales, Universidad de la Frontera, Temuco, Chile
[6]Center for Climate and Resilience Research, Universidad de Chile, Santiago, Chile
[7]Dirección General de Aguas, Ministerio de Obras Públicas, Chile
[8]Instituto Argentino de Nivología, Glaciología y Ciencias Ambientales (IANIGLA), CCT CONICET Mendoza, Argentina
[9]Centro de Estudios Avanzados en Zonas Áridas (CEAZA), La Serena, Chile
[10]Department of Civil Engineering, University of Chile, Santiago, Chile
[11]Advanced Mining Technology Center, University of Chile, Santiago, Chile
[12]Departamento de Recursos Hídricos, Universidad de Concepción, Campus Chillán, Chillán, Chile
[13]Sustainable Minerals Institute, The University of Queensland, Brisbane, Australia
[14]Centro de Investigación en Ecosistemas de la Patagonia, Coyhaique, Chile
[15]Waterways Centre, University of Canterbury, Christchurch, New Zealand
[16]Department of Civil Engineering, Universidad de la Frontera, Temuco, Chile

Correspondence to: Alexis Caro (alexis.caro.paredes@gmail.com), and Freddy Saavedra (freddy.saavedra@upla.cl)

https://doi.org/10.5194/essd-2026-324
Preprint. Discussion started: 12 May 2026

Open Access Earth System Science Data Discussions

Abstract.

The snowpack is a critical component of the water cycle in the Southern Andes of Chile and Argentina. In this region, quantitative assessments of snow accumulation remain limited by the scarcity, heterogeneity, and inconsistency of *in situ* observations, leading to large uncertainties in mountain hydrological modeling. To address this gap, we compile and quality–control snow depth observations, which are more spatially extensive and have a higher temporal resolution than snow water equivalent measurements, producing a consistent daily dataset of 81 stations between 21°S and 54°S for the period 2010–2024. Our quality-control procedure was primarily based on an adjustment of the snow depth ground reference level defined as the soil surface during snow-free periods, followed by the removal of anomalous spikes and observations outside physically plausible ranges. This process substantially improved data reliability, increasing the Physical Consistency Index (PCI), a multivariable metric that evaluates whether snow accumulation events are consistent with precipitation occurrence and lower temperatures, from 87 % to 95 % at some stations, while reducing the median data availability across all stations by 23 % (from 1,392 to 1,074 observations). The snow depth data availability increased markedly over time, from only one station in 2010, to 14 stations in 2015, and up to 57 stations in 2024, largely driven by expanded monitoring efforts of the General Directorate of Water, Chile. However, this expansion remains uneven across the Andean zones. The Mediterranean Andes concentrate the highest station density (39) and the largest number of highly complete records, with 17 stations reaching 80–100 % data coverage. In contrast, both the Arid Andes and the Wet Andes have only nine stations each reaching the same level of completeness, highlighting persistent spatial and temporal gaps. Using this newly quality–controlled dataset, we find that snow depth increases with precipitation from the Arid to the Wet Andes, but does not necessarily increase with elevation. The snow depth–elevation relationship is nonlinear in the Arid and Mediterranean Andes, with maximum accumulation at 4,300 m a.s.l. in the Elqui River Basin and 3,300 m a.s.l. in the Maipo River Basin. In contrast, a positive relationship emerges in the Wet Andes (Maule–Itata River Basin). This open–access, quality–controlled snow depth dataset (Medina and Caro, 2026, https://doi.org/10.5281/zenodo.20089265) represents the largest and most complete collection of continuous snow depth data for the Southern Andes, providing a robust basis for hydrological applications, such as model forcing and calibration, empirical analyses, reanalysis evaluation, and improved seasonal streamflow forecasting.

1 Introduction

Seasonal snowpacks are a key component of mountain hydrology, storing winter precipitation and releasing water during the dry season, thereby sustaining downstream water resources (Stewart et al., 2009). However, quantifying snow storage and its spatial variability remains challenging due to the limited availability and uneven distribution of *in situ* observations. This limitation is particularly pronounced in the Southern Andes (20° S–55° S), where long-term, quality-controlled observations of snow depth (SD) and snow water equivalent (SWE) remain scarce and fragmented across monitoring networks. In the Arid and Mediterranean Andes, the seasonal snowpack is a fundamental hydrological resource, providing water for human consumption and supporting ecosystems, agriculture, hydropower generation, and many industrial activities including mining (SERNAGEOMIN, 2021; Masiokas et al., 2020).

https://doi.org/10.5194/essd-2026-324
Preprint. Discussion started: 12 May 2026

The hydrological role of the seasonal snowpack varies across Andean climatic zones. In the Mediterranean Andes (31° S–36° S), seasonal and interannual streamflow variability of the main rivers is primarily controlled by snowmelt, with secondary contributions from glacier melt and minimal influence from rainfall. As a result, river discharge exhibits a relatively simple unimodal regime, with peak flows occurring in late spring and early summer (Masiokas et al., 2016, 2019; Burger et al., 2019; Ayala et al., 2020). In contrast, in the Wet Andes (36° S–55° S), snowmelt accounts for approximately 26 % of the annual runoff (Krogh et al., 2015) and rivers show more complex seasonal patterns influenced by precipitation events throughout the year. Compared to the Wet Andes, the Arid and Mediterranean Andes have experienced a prolonged megadrought since 2010, characterized by deficits in precipitation and a reduction in accumulated snow (Garreaud et al., 2017; 2020). This has led to reduced river discharges, decreasing water availability and intensifying conflicts over water rights as demand increasingly exceeds supply (Rivera et al., 2016; Álvarez–Garretón et al., 2021). Although glacier melt has partially buffered streamflow reductions during the ongoing megadrought, sustaining runoff despite significant precipitation deficits, this compensatory effect is associated with accelerated ice loss and is therefore expected to diminish in the future, potentially exacerbating water scarcity under prolonged dry conditions (Ayala et al., 2025; Caro et al., 2025).

SD and SWE are key variables for quantifying the hydrological contribution of the seasonal snowpack. While SWE is more directly linked to water storage than SD, obtaining SWE measurements is considerably more challenging than measuring SD. SWE can be measured directly or estimated by combining SD with measured or modeled snow density values (Ntokas et al., 2021). Specifically, the end–of–winter spatial distribution of SD and SWE are crucial for forecasting spring and summer streamflow in high mountain regions (Shaw et al., 2020a). However, because *in situ* snow observations are typically sparse and mostly located at low elevations, snow cover, SD and SWE are commonly obtained through spatial extrapolation supported by satellite imagery and modeling approaches (Cornwell et al., 2016; Cortés and Margulis, 2017; Shaw, et al., 2020a; Bulovic et al., 2025; Saavedra et al., 2026). In Chile, these limitations are further exacerbated for SWE, as observations are substantially more restricted than SD data in terms of spatial density and temporal coverage, with large data gaps.

SD monitoring networks in the Southern Andes have expanded in recent years, increasing spatial coverage across a wider range of latitudes and elevations. In Chile, the growing demand for spatially distributed snow information has driven government agencies and private entities to finance their expansion. The General Directorate of Water (Dirección General de Aguas, DGA) has consolidated national SD observations since 2010, while research institutions and universities, including the Centro de Estudios Avanzados en Zonas Áridas (CEAZA) and the Department of Civil Engineering at the Universidad de Chile (UdeChile), operate stations in the Arid and Mediterranean Andes. In the Wet Andes, monitoring efforts are led by the Centro de Estudios Científicos (CECs) and the Centro de Investigación en Ecosistemas de la Patagonia (CIEP). However, SWE observations from CEAZA, UdeChile, and CIEP are either unavailable or limited to short and discontinuous periods and, therefore, SWE records remain largely restricted to a small number of DGA stations. In Argentina, several institutions have expanded snow monitoring networks across the Andes, including the Instituto Argentino de Nivología, Glaciología y Ciencias Ambientales (IANIGLA), which has monitored SD variations near selected glaciers since 2014. Other institutions, typically responsible for water management at the provincial and regional levels, conduct SWE observations to support seasonal streamflow forecasts using automatic sensors (snow pillows, snow scales) and sporadic manual measurements at selected sites.

Publicly available SD data face challenges related to data acquisition, heterogeneous formats, and limited quality–control, which reduces their applicability for technical and scientific analyses. Across existing regional studies in the Southern Andes (Cornwell et al., 2016; Cortés and Margulis, 2017; Bulovic et al., 2025), the *in situ* observations are limited to only 12–26 sites and stations, mostly concentrated within a narrow latitudinal range of 32.4° S–34.8° S (25–75th percentile range) and at mid–elevation sites, approximately 2,500–3,600 m a.s.l. (25–75th percentile range). However, these datasets are used to extrapolate SD and SWE conditions across a much broader region (27° S–37° S), and to higher elevations above 4,000 m a.s.l., as snow accumulation at higher elevations are critical for water supply during the dry season (Masiokas et al., 2020).

This limited spatial and elevational coverage introduces substantial uncertainty in characterizing how snow depth varies with elevation. While some studies in the Southern Andes report positive SD–elevation gradients (Cornwell et al., 2016; Cortés and Margulis, 2017), evidence from other mountain regions suggests more complex, non-linear relationships, with SD increasing up to a peak and decreasing at the highest elevations due to precipitation patterns and snow redistribution processes such as

https://doi.org/10.5194/essd-2026-324
Preprint. Discussion started: 12 May 2026

wind transport, sloughing, and avalanching (Grünewald et al., 2014). These contrasting findings highlight the lack of observational constraints at high elevations and limit our ability to robustly assess snow storage across elevation gradients in the Southern Andes.

Despite valuable progress in SD and SWE observations across the Southern Andes, estimating SWE from basin to regional scales remains challenging due to a restricted observational record. Latitudinal and elevational sampling biases limit the representativeness of current datasets, directly impacting the reliability of regional simulations. These challenges are exacerbated by the lack of a coordinated framework to provide homogenized and quality-controlled SD data for the region. To date, no coordinated initiative has developed a homogenized, quality–controlled SD dataset. This hinders the understanding of the mountain hydrological cycle and the inherent variability that exists with elevation and across catchments throughout the Southern Andes. It also constrains accurate hydrological modeling, and reduces the reliability of climate change impact projections by hampering robust calibration and validation, particularly for extreme years within the historical records. Consequently, the lack of a quality–controlled SD dataset also limits the effective planning and management of current and future water resources under twenty–first–century climate change scenarios.

In this study, we provide the first daily, homogenized, quality-controlled SD dataset for the Southern Andes. The dataset covers the 2010–2024 period and integrates observations from automatic stations operated by government agencies, research centers, and universities across Chile and Argentina. A Quality–control procedure was conducted using a Python–based algorithm and consisted of four steps. The results are presented as daily quality-controlled SD observations at the station level. To demonstrate the scientific value of this dataset, we further analyze snow depth–elevation relationships across river basins and climatic zones, addressing a key but still uncertain aspect of snow accumulation patterns in the Andes. This comprehensive and consistent dataset is intended to improve model calibration and seasonal streamflow forecasting, as well as to enhance short- and long-term projections of water availability at local and regional scales under future climate change scenarios.

1.1 Study area

The Southern Andes is commonly divided into the Arid, Mediterranean, and Wet Andes (Saavedra et al., 2017; Caro et al., 2021). These zones are shown in Figure 1 for the range included in our study area between 21° S to 54° S, together with the distribution of the SD stations analysed in this study. In the northern Arid Andes, precipitation predominantly occurs during autumn (MAM) and winter (JJA). However, toward the northernmost sector of the Arid Andes, significant precipitation occur during summer (DJF), associated with the Bolivian Winter. At high elevations, air temperatures typically remain below freezing, reaching minimum values of −29 °C at Guanaco Glacier (5,324 m a.s.l., 2008–2011) (MacDonell et al., 2013). The Mediterranean Andes encompasses the most densely populated areas of Chile, which accounts for approximately 65 % of Chile's total population (Valparaíso to Ñuble Regions, INE, 2024), and important cities and industrial-agricultural areas in central-western Argentina. It also encompasses Chile's primary agricultural lands and supports the country's main electricity generation and irrigation infrastructure, contributing roughly 74 % of total agricultural lands of Chile in 2021 (INE, 2022). Further south in the Wet Andes, the mountain range transitions to a wetter climate influenced by Pacific frontal systems. Although mean monthly precipitation also peaks in autumn–winter, it remains substantial through spring–summer (SON-DJF), exceeding 150 mm/month (Lago Vargas station, 1977–1991), and is accompanied by comparatively warmer air temperatures (Dussaillant et al., 2012).

Across Chilean and Argentinean territories, the persistent snow covers 34,370 km² between 29° S and 36° S (Saavedra et al., 2018). Chilean mountain river basins generally drain westward to the Pacific Ocean, whereas those in Argentina drain eastward

https://doi.org/10.5194/essd-2026-324
Preprint. Discussion started: 12 May 2026

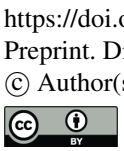

Open Access Earth System Science Data Discussions

to the Atlantic. Hydrological regimes vary latitudinally: southern basins are dominated by winter precipitation with secondary contributions from spring snowmelt, producing a pluvio-nival regime; in contrast, northern basins rely mainly on spring and early summer snowmelt and, to a lesser extent in the Chilean basins, winter precipitations, resulting in a mostly nival to nivo-pluvial regimes (Masiokas et al., 2019). These spatial patterns are governed by large-scale atmospheric circulation, as well as by latitudinal gradients, elevation, and local physiographic controls.

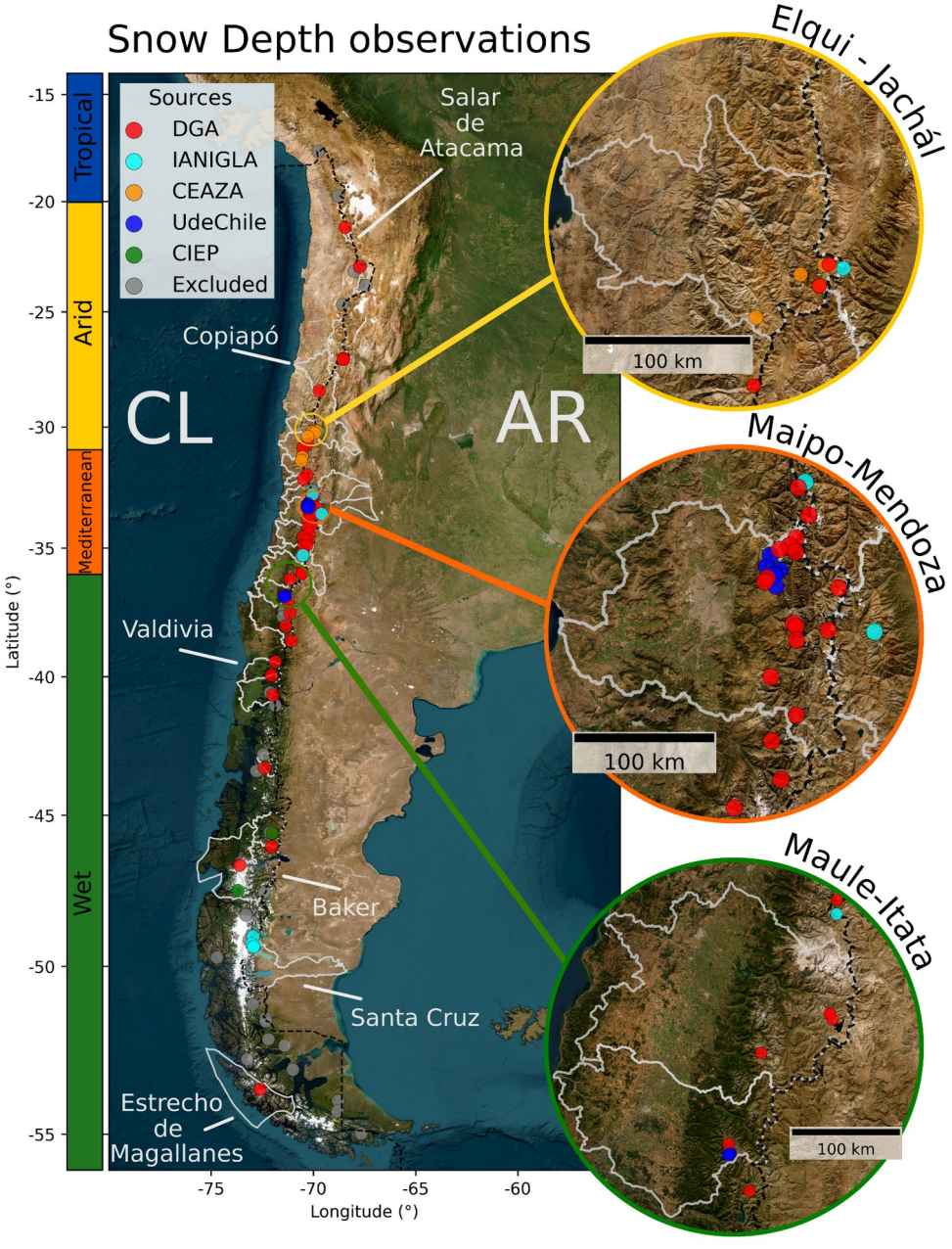

Figure 1. Spatial distribution of snow depth stations from 81 selected stations across 26 river basins and climate zones (Arid,

https://doi.org/10.5194/essd-2026-324
Preprint. Discussion started: 12 May 2026

Mediterranean, Wet) in the Southern Andes. Station locations from the institutional sources used in this study (DGA, IANIGLA, CEAZA, UdeChile, and CIEP) are shown, along with 37 excluded stations. Basemap imagery: Esri World Imagery © Esri, Maxar, Earthstar Geographics, and the GIS User Community | Powered by Esri.

2 Quality-control procedure

The complete quality–control procedure is summarized in the workflow shown in Figure 2. This procedure comprises four sequential steps, ranging from data compilation (Step 1) to cross-variable validation at the station level (Step 4). Following completion of the data processing and quality–control, SD–elevation relationships were analyzed at the river basin scale.

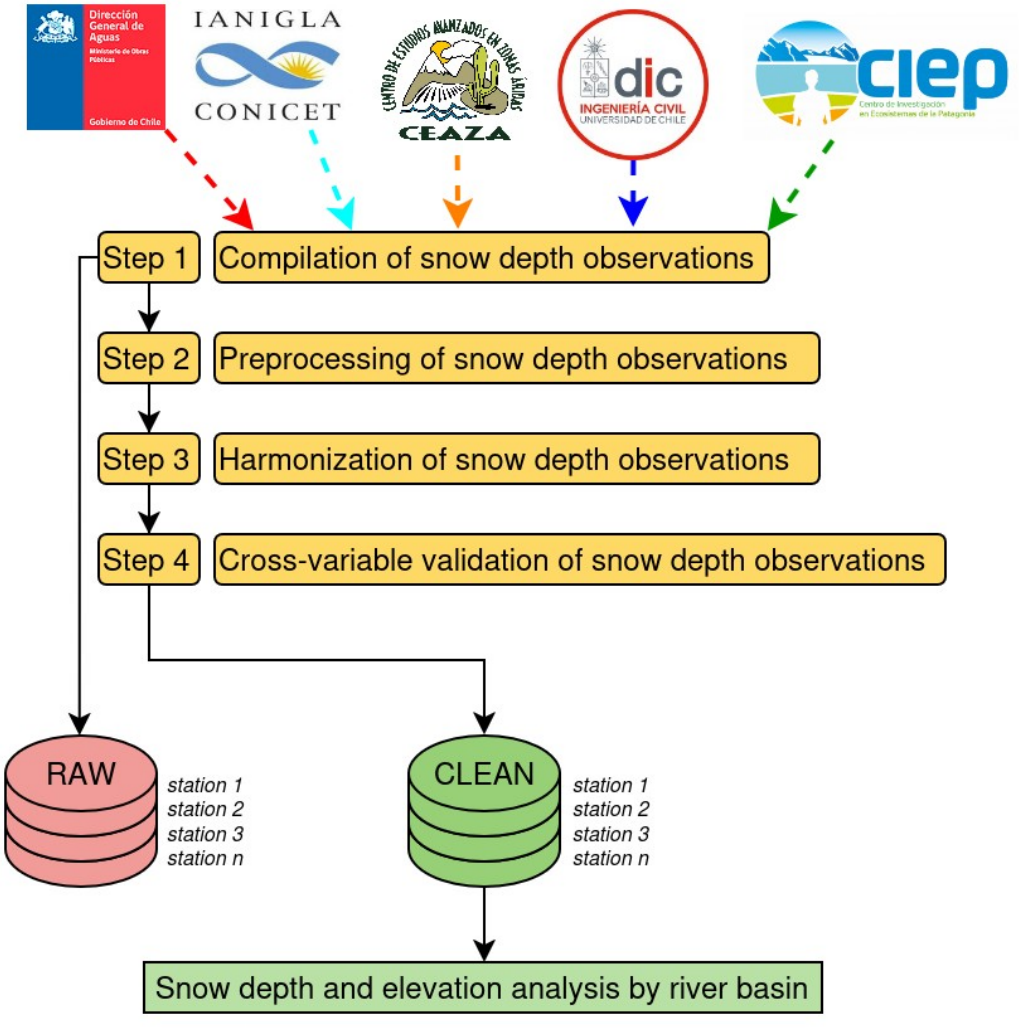

Figure 2. Workflow of the data processing and quality–control procedure applied to the 2010–2024 snow

https://doi.org/10.5194/essd-2026-324
Preprint. Discussion started: 12 May 2026

depth dataset across the Southern Andes, incorporating data from five different contributing institutions.

2.1 Step 1 – Compilation of snow depth observations

This study compiled data from 118 stations with SD observations distributed across the Southern Andes, between 17° S and 55° S. In addition, precipitation (Pr) and air temperature (AT) data were compiled to assess the physical consistency of the SD records in two river basins. Data were obtained from multiple institutions in Chile, including DGA, CEAZA, UdeChile, CIEP, and IANIGLA from Argentina.

SD observations were collected either through direct requests or by downloading publicly available datasets. The original data for Chile are available from https://snia.mop.gob.cl (DGA), https://www.ceazamet.cl (CEAZA), http://190.121.23.217/index_cdataaysen.php (CIEP) and Huerta et al., (2019). The data available for Argentina was provided by IANIGLA and is partially available from https://observatorioandino.com/estaciones/. Given the heterogeneous structure of these sources, the data were reorganized into a tabular format, with each column representing a monitoring station and each row containing the daily mean values for SD. This initial data compilation was consolidated into a "raw" file.

2.2 Step 2 – Preprocessing of snow depth observations

Prior to data cleaning of the "raw" file obtained in Step 1, an initial station-level screening was conducted to remove stations with inadequate data quality. Stations were deemed to have inadequate quality based on criteria used to evaluate data consistency, sensor performance, and record overlap. Following this procedure, 81 out of 118 stations with SD observations were selected, providing coverage across the Andes between 21° S and 54° S. The selected stations span elevations from 30 to 5,804 m a.s.l., and their records cover the period 2010–2024. Table 1 summarizes the main characteristics of the compiled SD dataset aggregated by river basin, while selected metadata for each station are provided in Table A1 in the Appendix.

A total of 37 stations were excluded from the subsequent analyses due to substantial data quality issues. These include unrealistically large day-to-day variations in SD (exceeding 1 m), insufficient record length at monthly and annual scales (in some cases with only a few days of observations per month), and limited temporal representativeness. In addition, several excluded stations correspond to recently available records (late 2025 and 2026) that do not yet provide sufficient temporal coverage for robust analysis. A complete list of excluded stations is provided in Table A2.

Table 1. Characteristics of snow depth stations by river basin across the Southern Andes (21° S–54° S). CL and AR refer to Chile and Argentina, respectively.

Andean zone	River Basin (Country)	N° Stations	Latitude (median, °S)	Station elevation (median, m a.s.l.)	Sources
Arid Andes	Salar Michincha (CL)	1	21.2	5,087	DGA
	Salar Atacama (CL)	1	23.0	5,625	DGA
	Tres Cruces (CL)	2	27.1	5,503	DGA
	Copiapo (CL)	1	28.5	3,985	DGA
	Jáchal (AR)	1	30.2	4,754	IANIGLA
	Elqui (CL)	7	30.2	3,660	CEAZA, DGA
	Limarí (CL)	3	30.9	3,529	DGA, CEAZA
	Choapa (CL)	2	31.7	3,432	CEAZA, DGA
Mediterranean Andes	Petorca (CL)	1	32.2	3,143	DGA
	Aconcagua (CL)	2	32.9	3,691	DGA
	Mendoza (AR)	2	33.2	3,544	IANIGLA
	Maipo (CL)	21	33.3	3,340	DGA, UdeChile

https://doi.org/10.5194/essd-2026-324
Preprint. Discussion started: 12 May 2026

	Rapel (CL)	7	34.7	2,665	DGA
	Mataquito (CL)	1	35.2	2,602	DGA
	Tunuyán (AR)	1	35.3	2,453	IANIGLA
Wet Andes	Maule (CL)	4	36.0	1,993	DGA
	Itata (CL)	5	36.9	1,809	UdeChile, DGA
	Biobio (CL)	5	37.6	1,784	DGA
	Valdivia (CL)	2	39.7	1,683	DGA
	Bueno (CL)	1	40.7	920	DGA
	Yelcho (CL)	1	43.3	575	DGA
	Aysén (CL)	2	45.6	1,310	CIEP, DGA
	Costeras e Islas R. Aisén R. Baker (CL)	1	46.7	1,187	CIEP, DGA
	Baker (CL)	2	46.8	555	DGA
	Santa Cruz (AR)	4	49.3	984	IANIGLA
	Islas sur Estrecho de Magallanes (CL)	1	53.7	70	DGA

A series of automated algorithms were implemented using the Pandas library (The pandas development team, 2025) to adjust the ground reference level (corresponding to the soil surface and established after sensor installation or maintenance), to correct anomalous spikes, and to remove implausible or extreme values. For these procedures, stations were grouped by river basin and processed collectively using shared parameters and thresholds calibrated for each basin, as detailed below. In addition to this basin-level processing, a supplementary manual filtering step was applied on a station-by-station basis. This step, based on expert judgment, was used to identify and remove residual localized outliers not captured by the automated procedures, thereby ensuring the overall reliability of the dataset.

Step 2.1. Zero-level correction: This step realigns the SD ground reference level to account for instrumental drift during snow-free periods. The algorithm identifies abrupt changes by assessing variability in the SD time series using a moving-window range, defined as the difference between the maximum and minimum SD values within each window. Across the three Southern Andean zones, a median window length of five days was adopted, with river basin-specific adjustments ranging from three to five days. A period is classified as stable if the SD moving range falls below the sensor noise threshold for SD measurements (1 cm). To ensure that actual snowpacks are not erroneously corrected, stable windows (as defined by the SD moving range) with median SD values exceeding a predefined snow threshold (5 cm) are preserved. Conversely, if the estimated offset corresponds to a stable window (i.e., SD moving range < 1 cm) and falls within a near-zero tolerance limit (0.5 cm), it is treated as regular SD sensor noise and set exactly to zero. Then, to preserve continuity and avoid constant micro-adjustments, the validated offset (defined as the offset estimated from stable, snow-free windows after applying the tolerance criteria), is subtracted from all subsequent SD observations only if it deviates from the previously established ground reference level by more than a drift tolerance of 0.5 cm. While the SD sensor accuracy is ±1 cm (https://www.campbellsci.com/sr50a), this analysis relies on daily averages derived from high-frequency (hourly) SD observations, further aggregated using a multi-day sliding window. This temporal averaging substantially dampens random noise and reduces the statistical uncertainty of the estimated ground reference level. This reduction in variance justifies the use of a stricter threshold (0.5 cm) for the tolerance limits applied in the correction procedure, enabling the detection of subtle systematic shifts that would otherwise be obscured by the manufacturer's nominal instrumental error.

Step 2.2. Spike removal: To identify and remove isolated spikes in SD time series related to each station, the median absolute deviation (MAD, Rousseeuw & Croux, 1993) was applied using a centered moving window (3 to 15 days) tailored to each basin's SD variability. The median window size (ω) was three days in the Arid Andes, nine days in the Mediterranean Andes, and six days in the Wet Andes. For a given day t ,the MAD is calculated as:

https://doi.org/10.5194/essd-2026-324
Preprint. Discussion started: 12 May 2026

Open Access Earth System Science Data Discussions

$$MAD_t = \text{median}_w\left(|SD_i - \widetilde{SD}_t|\right) \quad \text{Equation 1}$$

where SD_i represents the daily observation within the sliding window ω centered at day t, and $\widetilde{SD}_t$ is the median of that window.

A daily observation was flagged as a spike and removed if it met either of two independent criteria. The first criterion evaluated deviations from the window median using a scaling factor, k. Conceptually, k acts as a tolerance threshold that defines the acceptable range of natural variability around the median. Because snow accumulation is inherently irregular, k was calibrated based on the observed behavior at each station within the river basin, with values ranging from 2 to 7. The median value of k was 4 in the Arid and Mediterranean Andes and 6 in the Wet Andes. To avoid inadvertently removing true extreme snowfall events, this criterion required that any suspected spike exhibit clear discontinuities (> k · MAD) relative to both adjacent days. Additionally, the absolute difference between the two adjacent days had to remain small (< k · MAD), confirming that the event represented an isolated anomaly rather than a sustained change in SD. The second criterion acted as an absolute physical filter. Regardless of MAD, an observation was flagged and removed if the absolute difference compared to both adjacent days exceeded a fixed, extreme physical magnitude, depending on SD variability of its respective basin. The median value of this threshold was 75 cm in the Arid, 100 cm in the Mediterranean, and 140 cm in the Wet Andes.

Step 2.3. Physical range check: A physical range filter was applied to the SD time series at each station.

Lower and upper plausible limits were defined for each river basin based on station elevation, regional climatology, and expert knowledge. Observations below the ground reference level were set to zero, whereas values exceeding the upper physical limit were considered implausible and removed. The median physical limits were 0–140 cm in the Arid Andes, 2–360 cm in the Mediterranean Andes, and 2–300 cm in the Wet Andes. The lower limit in the Mediterranean and Wet Andes was set to 2 cm to account for sensor noise (±1 cm) and local surface roughness (e.g., low vegetation or rocky terrain). Setting these near-zero values to zero prevents instrumental and surface-related noise from being misinterpreted as shallow snow accumulation.

The output of this step is a cleaned SD file that preserves the structure of the original raw SD dataset while containing quality–controlled values for each monitoring station.

2.3 Step 3 – Harmonization of snow depth observations

When overlapping daily SD observations exist for the same station due to data being compiled from multiple sources, a single unified time series is constructed. For example, the DGA dataset for some stations may include multiple versions of the same SD observation, arising either from data updates or from the incorporation of post-processed information obtained from external sources for specific stations. The unified time series is the one with the highest data availability and the strongest Pearson correlation with nearby stations during the overlapping period. This step is crucial for ongoing updates to the quality–controlled SD dataset after publication, as revised data releases may differ from earlier versions for the same dates by station. Such differences may arise from technical decisions by data providers or from sensor replacements affecting SD observations.

2.4 Step 4 – Cross-variable validation of snow depth observations

A multivariable validation procedure was applied to assess the physical consistency of both raw and quality-controlled SD observations. The analysis was restricted to stations located in the Elqui and Maipo River Basins with overlapping daily

https://doi.org/10.5194/essd-2026-324
Preprint. Discussion started: 12 May 2026

Open Access Earth System Science Data Discussions

observations of SD, Pr, and AT during the May–October period, corresponding to the snow accumulation season in the Southern Andes (Masiokas et al., 2020; Bulovic et al., 2025). The approach is based on the joint physical consistency among these variables. Snow accumulation, defined as a positive day-to-day change in SD (positive ΔSD), is expected to occur during precipitation events under sufficiently cold air temperature conditions. In contrast, snow ablation (negative ΔSD) may result from multiple processes (e.g., melt, sublimation, compaction, or wind redistribution), which are not directly observed at most weather stations. Due to these uncertainties, only snow accumulation events were evaluated.

The new Physical Consistency Index (PCI) was developed and implemented to classify each day as physically consistent ($\phi i = 1$) or inconsistent ($\phi i = ¿$ 0), following a multivariable framework inspired by the Perkins Skill Score (PSS, Perkins et al. 2008) and the Automated Quality assurance of daily surface observations procedures (AQ, Durre et al., 2010). First, to reduce the influence of measurement noise in ΔSD, a station-specific threshold (τ) was defined as the 5th percentile of the positive ΔSD distribution. When τ was lower than 1 cm, corresponding to the sensor accuracy, it was set to this minimum value. A day was classified as a potential snow accumulation event only when ΔSD > τ; all other days (ΔSD ≤ τ and ΔSD = 0) were excluded from further analysis. Second, to ensure physical consistency with meteorological conditions, only days with measurable precipitation (Pr > 1 mm) were retained, reducing uncertainties associated with gauge undercatch and wind-driven snow redistribution. For these events, an air temperature threshold (AT_{rain}) was defined as the 95th percentile of AT at each station. Accumulation days with AT exceeding this threshold were classified as physically inconsistent ($\phi i = ¿$ 0), whereas those with AT below the threshold were considered physically consistent and retained as valid snow accumulation signals ($\phi i = ¿$ 1).

The PCI for each station was calculated as the ratio between the number of physically consistent snow accumulation days ($\phi i = ¿$ 1) and the total number of identified snow accumulation days with Pr > 1 mm (N). This index is defined in Equation 2, where ϕi is a binary consistency indicator for each day i, taking a value of 1 for physically consistent conditions and 0 otherwise.

$$PCI = \frac{1}{N}\sum_{i=1}^{N}\phi_i \quad , \qquad \text{Equation 2}$$

where ϕ_i is the consistency indicator for each *i* daily snow accumulation day, defined as:

$$\phi_i = \begin{cases} 1, & \text{if } (\Delta SD_i > \tau) \wedge (Pr_i > 1\,\text{mm}) \wedge (AT_i \leq AT_{rain}) \\ 0, & \text{otherwise} \end{cases}$$

While the PCI provides a relative measure of the physical consistency of snow accumulation events, its interpretation in isolation can be misleading. As a ratio, highly noisy raw SD observations may artificially inflate PCI values, in some cases making them comparable to or even higher than those derived from the quality–controlled SD dataset. To complement the PCI, two additional metrics were developed in this study and computed using the same event definition and filtering criteria described in Equation 2. First, the Net Inconsistency Reduction (ΔE) is defined in Equation 3 as the difference between the number of physically inconsistent days detected in the raw (N_{raw}) and quality–controlled SD datasets (N_{QC}), with positive values indicating a reduction in inconsistencies. Second, the Noise Ratio (NR) is defined in Equation 4 as the proportion of the total number of apparent accumulation events detected in the raw dataset ($N_{event,raw}$) to the number of events retained after quality–control ($N_{event,QC}$). Values of NR greater than 1 indicate that the procedure effectively identified and removed spurious positive SD spikes, revealing the presence of noise or measurement artifacts in the raw SD dataset.

https://doi.org/10.5194/essd-2026-324
Preprint. Discussion started: 12 May 2026

$$\Delta E = N_{raw} - N_{QC}\,, \qquad \text{Equation 3}$$

$$NR = \frac{N_{event,raw}}{N_{event,QC}} \qquad \text{Equation 4}$$

2.5 Snow depth and elevation analysis by river basin

Due to the limited temporal continuity of SD observations across stations located at different elevations and in different river basins for the same dates, the observations were grouped into three precipitation year types. Based on precipitation records from the General Directorate of Water (DGA) and the Dirección Meteorológica de Chile (DMC), we identified, for three basins, years representative of different ranges of total annual precipitation: dry [0th to 30th percentile], normal (30th to 70th percentile], and wet (70th to 100th percentile] (Table A3). For the Elqui, Maipo, and Maule–Itata River Basins, we selected precipitation observations from stations at relatively high elevations: La Laguna Embalse station (3,160 m a.s.l.) in the Elqui River Basin; 19 stations in the Maipo River Basin; and the Diguillín (670 m a.s.l.), Río Diguillín en San Lorenzo–Atacalco (727 m a.s.l.), and Las Trancas (1,242 m a.s.l.) stations in the Maule–Itata River Basin. These basins were selected because they contain a sufficient number of SD observations with a well-distributed elevation range.

A positive correlation between elevation and precipitation is generally expected, reflecting the influence of orographic enhancement of precipitation (Scaff et al., 2017). In contrast, mean air temperature is expected to exhibit a negative correlation with elevation, with lower mean temperatures typically observed at higher elevations (Voordendag et al., 2021; Aguayo et al., 2024; Caro et al., 2024). To quantify the combined effect of these competing processes, the SD–elevation relationship was analyzed using the 25th, 50th, and 75th percentiles, as well as the cumulative distribution function (CDF), across three precipitation year types, providing a robust basis for comparing SD across elevations and contrasting climate conditions in the Andean zones.

To analyze the SD–elevation relationship, only stations with at least 70 % of daily SD data availability per month during the accumulation period (1 May to 31 October) were retained, and elevation was derived from the 30 m SRTM digital elevation model. This approach enabled consistent comparison of SD observations across elevations within each precipitation year type.

Additionally, the median snow line elevation in July, as well as its 25th percentile, was estimated for these three river basins using satellite-derived snow persistence for the period 2000–2024. July corresponds to the month with the lowest snow line elevation in the year. Monthly snow persistence was derived from daily MODIS Terra and Aqua snow products (MOD10A1/MYD10A1, Collection 6.1; 500 m spatial resolution), processed in Google Earth Engine and reported by Saavedra et al. (2026). Snow presence (1) and absence (0) were defined using a normalized difference snow index (NDSI) threshold of 0.4. Elevation was obtained from the 30 m SRTM digital elevation model. The snow line elevation was defined as the contour where snow persistence equals 5%, and its elevation was calculated by intersecting this contour with the DEM and taking the median of the corresponding elevations.

3 Results

3.1 Snow depth measurements across the southern Andes

SD observations are available from 81 stations distributed across 26 river basins between 21° S and 54° S, covering the period 2010–2024. The Mediterranean Andes host the largest number of stations (39 stations in 7 basins), followed by the Wet Andes (28 stations in 11 basins) and the Arid Andes (18 stations in 8 basins). Despite this spatial distribution, the temporal availability

https://doi.org/10.5194/essd-2026-324
Preprint. Discussion started: 12 May 2026

of observations shows a marked increase over time. From 2015 onwards, the number of stations reporting SD data increases substantially, with a relatively steady growth until 2022, followed by a period of relative stabilization through 2024. Over the full study period, the SD observational network is primarily sustained by the DGA (52 stations), followed by the UdeChile (12 stations), IANIGLA (eight stations), CEAZA (seven stations), and the CIEP (two stations). These institutions exhibit distinct spatial coverage patterns. The DGA and IANIGLA provide the broadest geographical coverage across Chile and Argentina, respectively. In contrast, CEAZA is concentrated in the Elqui, Limarí, and Choapa River Basins within the Arid Andes; the UdeChile operates mainly in the Mapocho and Itata River Basins across the Mediterranean and Wet Andes; and the CIEP is focused on the Aysén and Baker River Basins in the Wet Andes.

Figure 3 presents the years with SD observations across the 81 stations of our final quality–controlled snow depth dataset, considering records from May to October over the period 2010–2024. Prior to 2015, SD observations were sparse and almost exclusively provided by the DGA, with only eight stations reporting data, predominantly located in the Mediterranean Andes (5 stations). Between 2015 and 2022, the network expands considerably from 14 to 52 stations with SD observations. This increase is still concentrated in the Mediterranean Andes (24 stations), largely driven by DGA, but also reflects the incorporation of additional data sources, including UdeChile (eight stations) and IANIGLA (three stations). In parallel, the Arid Andes show a notable increase in coverage, from zero stations prior to 2015 with 12 stations, mainly operated by DGA (six stations) and CEAZA (five stations). In contrast, the Wet Andes remain comparatively underrepresented throughout this period, with the number of SD observations increasing from seven in 2015 to 16 in 2022, despite their substantially larger spatial extent relative to the other Andean zones.

In the most recent period from 2023–2024, the SD observational network reached its maximum spatial extent, with up to 57 stations reporting SD observations in 2024 across the Andes. This expansion is primarily driven by a substantial increase in stations operated by DGA in both the Arid and Wet Andes. In 2024, 25 stations report SD observations in the Mediterranean Andes, of which 22 are operated by DGA, while two stations correspond to IANIGLA and one to CEAZA. In the Arid Andes, 13 stations report SD observations, of which nine are operated by DGA. In the Wet Andes, 19 stations report SD data, with 16 operated by DGA. By 2024, the DGA plays a dominant role in the recent expansion of the station's network, including the incorporation of SD observations at the northernmost and southernmost limits of the Southern Andes.

In addition to the expansion of the SD observational network in 2024, further observational potential arises from stations recently installed or upgraded during 2025 and 2026, as well as from stations currently affected by measurement inconsistencies that are expected to be resolved in the near future (Table A2). This indicates that the effective availability of SD observations is likely to continue increasing beyond the period analysed here. Conversely, a subset of stations corresponds to short-term deployments associated with specific research projects. These stations typically provide observations over limited time windows and contribute to characterizing SD conditions during particular years only. As such, they fall outside the core long-term monitoring network, which is primarily sustained by the DGA and IANIGLA.

In terms of SD data availability, Figure 3 also describes the percentage of days with data from 0 to 100 % in the period May to October. Across the 81 stations of our final SD dataset, the year-by-year analysis of data availability reveals marked differences among the Arid, Mediterranean, and Wet Andes in terms of both data completeness and temporal continuity. In the Arid Andes, only six stations achieve high data availability, with SD observations covering 80–100 % of days per year for at least five years. Among them, Quebrada Larga (DGA) and La Laguna (CEAZA) exhibit the highest data availability, followed by Capayán (IANIGLA). The number of stations achieving 80–100 % annual data availability increases markedly to 17 in the Mediterranean Andes. The highest data availability corresponds to DGA stations, with continuous 11 year records at Laguna Negra and Olivares Gamma, followed by Portillo station. These stations also exhibit the longest temporal coverage, in addition to the Laguna Los Cristales and Termas del Flaco stations. Further south, in the Wet Andes, only six stations achieve 80–100 % annual data availability for at least five years. Among them, Lo Aguirre (DGA) stands out as the station with the longest record in the Southern Andes, beginning in 2010, followed by Nevado de Longaví (DGA) in 2011 and Aonikenk (IANIGLA) in 2014. Notably, continuous records of at least nine years are observed at Volcán Chillán and Alto Mallines stations.

https://doi.org/10.5194/essd-2026-324
Preprint. Discussion started: 12 May 2026

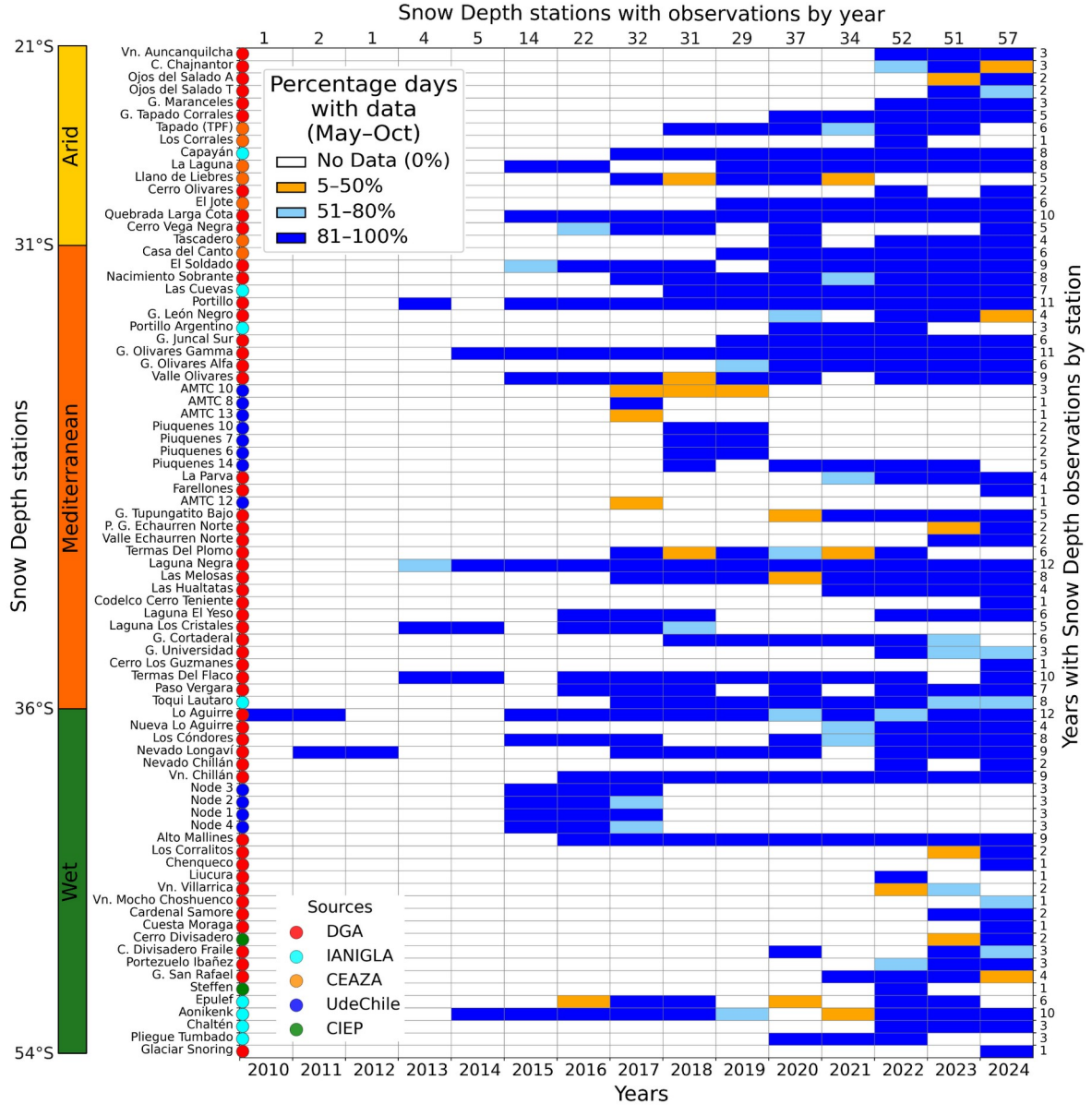

Figure 3. Availability of quality–controlled daily snow depth observations for 81 stations in Chile and Argentina (21°–54° S) from 2010 to 2024. Stations are sorted latitudinally from north to south. Colors indicate the annual percentage of days with available snow depth observations, based on daily records aggregated over the May–October period.

Figure 4 presents the daily SD observations in key places along the Southern Andes for the 2010–2024 period. SD observations show a consistent increase from the arid to the wet zones of Chile, in agreement with the corresponding gradient in total precipitation (Sarricolea et al., 2017). In the Arid Andes, north of 27° S, the high-elevation stations of Ojos del Salado and Cerro Chajnantor (both above 5,600 m a.s.l.) exhibit limited snow accumulation, primarily concentrated during the austral

https://doi.org/10.5194/essd-2026-324
Preprint. Discussion started: 12 May 2026

summer. In contrast, Tapado station (30° S, 4,300 m a.s.l.), located further south, shows larger snow accumulation predominantly during the winter season. This contrast highlights a marked difference in the seasonal timing of snow accumulation within the same Andean zone. In the Mediterranean Andes, stations located in the Aconcagua and Maipo River Basins exceed 200 cm of SD, with Las Melosas station (33° S, 3,300 m a.s.l.) reaching values above 300 cm. Despite the high precipitation that occurs in the Wet Andes (Sarricolea et al., 2017), the possible predominance of rainfall over snowfall, combined with warmer mountain temperatures compared to those observed further north during the winter months, limits snow accumulation. As a result, SD values during recent years are close to 200 cm at the Volcán Chillán station (37° S, 2,000 m a.s.l.), and reach around 150 cm east of the Southern Patagonian Icefield at the Aonikenk station (49° S, 1,200 m a.s.l.).

A clear west–east gradient is observed across the Andes, with higher SD values on the western side compared to the eastern side, due to the influence of moist air masses from the Pacific Ocean that produce greater precipitation over Chile than Argentina (Viale and Nuñez, 2011). In the Arid and Mediterranean Andes, at latitudes where both Chilean and Argentine SD stations are available, stations located on the western side of the Andes show higher SD values than those on the eastern side. For example, stations in the Elqui River Basin present SD values exceeding 50 cm between 2018 to 2021, whereas stations in the Jáchal River Basin almost not exceed this threshold, even for stations located above 4,000 m a.s.l. (Tapado TPF and Capayán). A similar pattern is observed in the Aconcagua and Maipo river basins compared to the Mendoza River Basin. However, this contrast in snow accumulation is not evident in the Wet Andes, where San Rafael station located on the western side of the Andes and Condón Divisadero and Aonikenk stations located on the eastern side show similar SD values during 2022 to 2024, at latitudes where the occurrence of rainfall strongly influences snow accumulation.

The effect of the megadrought in the Chilean Central Andes between 2010 and 2021 (Garreaud et al., 2025) can be seen in the SD observations, including a marked recovery of SD since 2023. Particularly, extremely dry conditions in 2019 and 2021 are evident, with SD stations located in the Aconcagua, Maipo, and Mendoza river basins above 3,000 m a.s.l. showing reduced SD values. This signal is also identifiable in stations within the Maule and Itata river basins.

https://doi.org/10.5194/essd-2026-324
Preprint. Discussion started: 12 May 2026

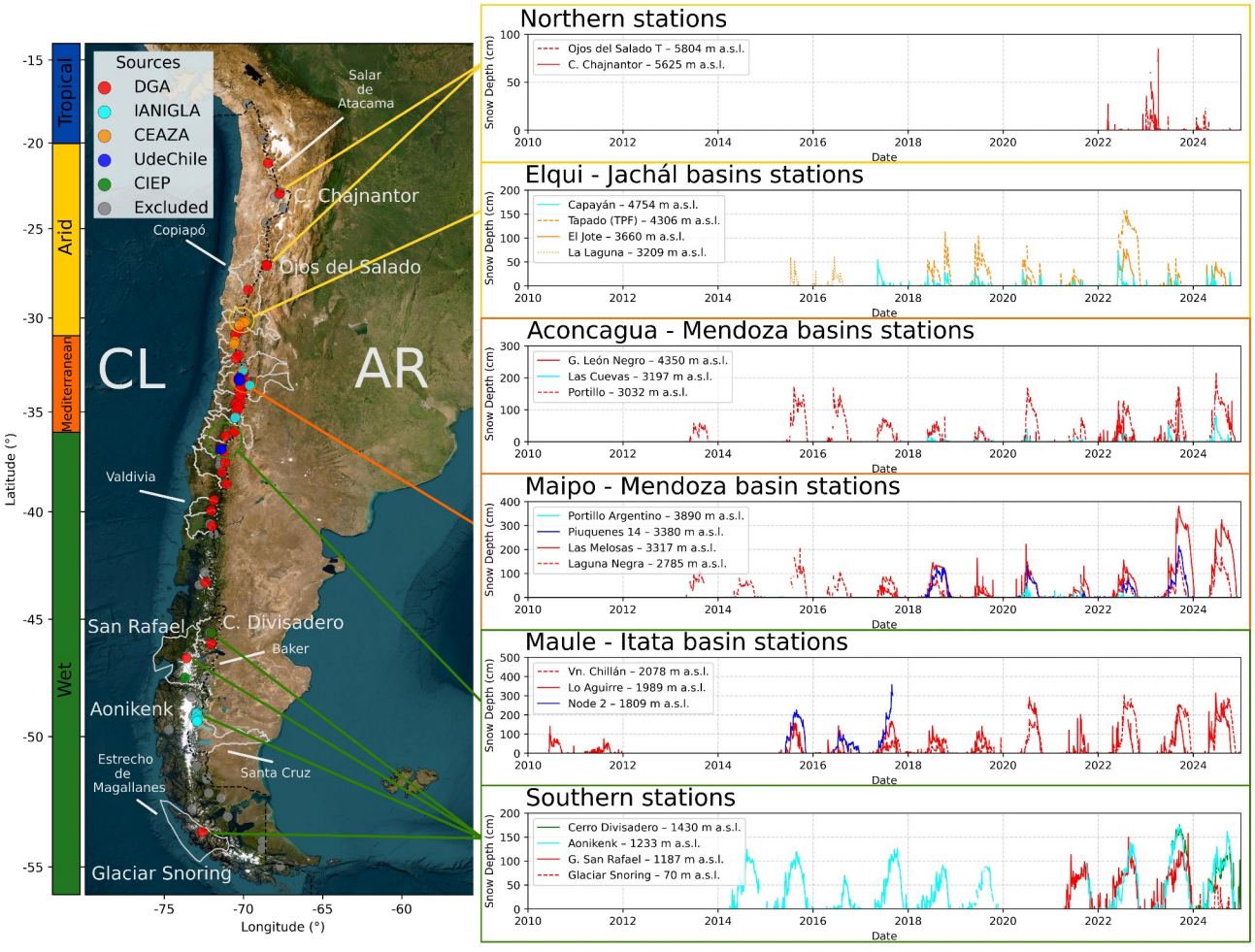

Figure 4. Spatial distribution of daily snow depth observations across the Southern Andes of Chile (CL) and Argentina (AR) between 21° S and 54° S, in main river basins and locations for the 2010–2024 period. The map shows station locations from multiple institutions, related to the Andean zones, spanning the transition from the arid northern Andes to the wet region of Patagonia. The snow depth time series in each panel illustrate the combined interannual and seasonal variability of snow conditions, as well as periods with data gaps. The vertical scale is different for each panel. Basemap imagery: Esri World Imagery © Esri, Maxar, Earthstar Geographics, and the GIS User Community | Powered by Esri.

3.2 Snow depth data availability: comparison of raw and quality-controlled versions

This section evaluates the quality of daily SD observations in both the raw and quality-controlled datasets over the 2010–2024 period. Table 2 summarizes the effective number of days with available SD observations and the relative data availability, defined as the proportion of days with data between the first and last available records, for both raw and quality-controlled datasets across 26 river basins spanning 21° S to 54° S. Details by station are shown in Table A4.

https://doi.org/10.5194/essd-2026-324
Preprint. Discussion started: 12 May 2026

Overall, a strong positive correspondence is observed between raw and quality-controlled effective days with data ($R^2 = 0.8$), indicating that the quality–control procedure preserves the relative ranking of stations in terms of data availability. No clear latitudinal dependence is identified in the reduction of data availability after cleaning. However, substantial basin-scale differences emerge. The largest median reductions in data availability (>50%) are concentrated in basins of the Wet Andes, including Valdivia (73%), Biobío (63%), Baker (58%), and the Costeras e Islas R. Aisén R. Baker (55%). These basins also exhibit relatively high initial data availability, suggesting that the quality–control procedure removes observations identified as inconsistent or exhibiting unusually high variability based on statistical and manual criteria.

The Vn. Mocho Choshuenco station largely explains the substantial number of SD observations filtered after applying the quality–control procedure in the Valdivia River Basin, as SD observations for the 2019–2022 period exhibit high dispersion that prevents both automated procedures and manual inspection from clearly identifying the seasonal snow accumulation cycle. In particular, the absence of a ground reference level associated without snow accumulation hinders the detection of low SD variability, leading to a large proportion of data being classified as unreliable and subsequently removed. Similar challenges are observed in the Biobío River Basin, especially at the Chenqueco and Liucura stations, where several months in 2023 at Chenqueco were discarded due to very low SD values (<2 cm) that could not be reliably attributed to persistent snow cover, resulting in the retention of only the 2024 observations, while at Liucura only 2022 SD observations were preserved because the 2023–2024 period exhibited irregular autumn–winter accumulation patterns, anomalously high SD values during the summer of 2024, and the absence of a consistent ground reference level. A comparable situation is found in the Baker River Basin and Costeras e Islas R. Aisén R. Baker, where the large reduction in SD observations is mainly explained by two out of three stations. At Steffen station, although data are available for 2020–2024, the very limited variability (<5 cm) prevents the identification of a clear seasonal cycle, with only a potential accumulation signal in 2022 reaching approximately 250 cm, whereas at G. San Rafael station, despite data availability from 2015 to 2024, the 2015–2019 period was excluded because accumulation and ground reference level months could not be distinguished, as illustrated by years such as 2016 and 2019, when higher SD values occur during spring (SON) and summer (DJF), which is inconsistent with the expected seasonal cycle in the Southern Hemisphere.
Intermediate reductions of days with data after cleaning (20–50 %) are observed in several basins across all climatic zones, notably Rapel River Basin (48 %) in the Mediterranean Andes and Limarí River Basin (48 %) in the Arid Andes, indicating that data loss is not exclusively controlled by latitude but is instead strongly influenced by station-specific issues. In the Rapel River Basin, the large proportion of SD observations failing the quality–control procedure is primarily associated with three stations: Laguna El Yeso, Laguna Los Cristales, and G. Universidad. Different sources of inconsistency are identified. At Laguna El Yeso, data from 2013 and 2015 were excluded due to the absence of snow accumulation during expected winter months, the lack of a consistent ground reference level, and highly incomplete records limited to isolated spring–summer periods between 2019 and 2021. At Laguna Los Cristales, SD observations from 2021 to 2024 were removed due to the absence of variability in the SD time series. However, at the G. Universidad station data from 2017 to 2021 were excluded due to high short-term variability in SD observations over consecutive days; nevertheless, a more detailed, station-specific analysis could potentially recover a substantial number of valid observations. A comparable situation is observed in the Limarí River Basin, where data exclusion is restricted to the Cerro Vega Negra station (2015 and 2021–2023), driven by abrupt SD variations from near 0 to approximately 200 cm within 1–2 days, likely reflecting inverted or mis-scaled observations (e.g., meters instead of centimeters), which, despite being partially captured by the quality–control procedure, can still be misinterpreted as valid snow accumulation periods and are therefore removed.

In contrast, minimal reductions in the number of days with data after quality–control procedure (< 1%) are observed in basins with only one station, such as Yelcho, Bueno, and Tunuyán river basins. Notably, the Elqui and Maipo river basins, despite having the highest station densities (7 and 21 stations, respectively), also exhibit very low median reductions (< 2%). This indicates a high potential for SD analyses in these basins, supported by the combination of dense observational networks and consistently high-quality records relative to other basins across the Southern Andes.

Out of the 81 SD stations of our final quality–controlled dataset, 45 stations distributed between 21° S and 49° S show reductions in data availability below 10%, with a median of 1,236 days with valid observations, after quality–control procedure. Within this group, the Elqui River Basin includes five stations, Glaciar Tapado en Los Corrales, Tapado (TPF), Los

https://doi.org/10.5194/essd-2026-324
Preprint. Discussion started: 12 May 2026

Corrales, La Laguna, and El Jote, while the Maipo River Basin comprises 11 stations: Glaciar Juncal Sur, Glaciar Olivares Gamma, Glaciar Olivares Alfa, AMTC10, Piuquenes7, La Parva, Farellones, AMTC12, Laguna Negra, Las Melosas, and Las Hualtatas. These results further highlight the robustness and spatial representativeness of SD observations in these basins.

Table 2. Effective days of snow depth observations for raw and quality-controlled datasets by river basin, considering all available records over the 2010–2024 period.

Basin (country)	N° Stations	Raw data		Clean data		Reduction of days with data after cleaning (%)	Total basin area (km²)
		Effective days with data (median)	Relative data availability (%)	Effective days with data (median)	Relative data availability (%)		
Salar Michincha (CL)	1	1,085	96	1,062	94	2	2,674
Salar Atacama (CL)	1	733	71	622	60	15	5,307
Tres Cruces (CL)	2	592	81	537	74	9	15,618
Copiapo (CL)	1	988	100	975	99	1	18,703
Jáchal (AR)	1	2,933	100	2,892	99	1	32,318
Elqui (CL)	7	1,769	84	1,742	83	2	9,825
Limarí (CL)	3	2,940	82	1,536	47	48	11,696
Choapa (CL)	2	2,720	97	2,596	92	5	7,653
Petorca (CL)	1	2,831	97	2,638	90	7	1,988
Aconcagua (CL)	2	2,825	95	2,297	77	19	7,334
Mendoza (AR)	2	1,866	100	1,809	99	3	21,830
Maipo (CL)	21	1,261	51	1,236	50	2	15,273
Rapel (CL)	7	2,461	57	1,282	53	48	13,766
Mataquito (CL)	1	2,910	90	2,145	66	26	6,332
Tunuyán (AR)	1	2,560	89	2,529	89	1	22,195
Maule (CL)	4	3,636	83	2,736	63	25	21,052
Itata (CL)	5	1,016	100	977	96	4	11,326
Biobío (CL)	5	1,129	99	419	38	63	24,369
Valdivia (CL)	2	1,081	75	296	62	73	10,244
Bueno (CL)	1	598	95	592	94	1	15,366
Yelcho (CL)	1	248	99	247	99	0	4,084
Aysén (CL)	2	1,112	93	762	63	32	11,456
Costeras e Islas R. Aisén R. Baker (CL)	1	2,567	75	1,149	83	55	35,153
Baker (CL)	2	1,354	99	573	96	58	20,945
Santa Cruz (AR)	4	1,490	61	1,313	57	12	29,938
Islas sur Estrecho de Magallanes (CL)	1	414	100	285	99	31	27,931

3.3 Assessing the physical consistency of snow depth with precipitation and air temperature by station

Table 3 summarizes the results of the PCI metric applied to stations located in the Elqui and Maipo river basins, which have the largest number of SD stations and the most comprehensive elevation distribution among the 26 river basins analyzed in this study. Two and five SD stations met the conditions required for this validation in Elqui and Maipo river basins, respectively, including overlapping daily SD, Pr, and AT data during the accumulation period (May–October) over the period 2017 to 2024, and satisfy the three criteria related to air temperature threshold, snow accumulation, and precipitation events (see in Section 2.4 Step 4). These strict data availability requirements resulted in a substantial reduction in the number of analyzed days, dropping from a median value in days with three variables overlap from the quality–controlled data of 896 to 19 analyzed days with PCI in Elqui River Basin and from 1,907 to 79 analyzed days in Maipo River Basin. This reduction is primarily explained as the filter explicitly isolates precipitation-driven accumulation days, discarding the majority of the winter season characterized by zero precipitation, stable snowpacks, or ablation periods. Complete results for both the raw and quality-controlled datasets are provided in Tables A5 and A6.

https://doi.org/10.5194/essd-2026-324
Preprint. Discussion started: 12 May 2026

Open Access Earth System Science Data Discussions

Across the analyzed stations, the quality–control procedure improves the stability of physical consistency metrics. In the Elqui River Basin, the PCI in the quality–controlled dataset ranges between 90.0 % and 92.9 %, compared to 90.5 % and 93.9 % in the raw dataset, indicating only minor changes in the spread of values after cleaning. In contrast, in the Maipo River Basin, the PCI range narrows substantially after quality–control, converging to 94.4%–94.9 % from a wider range of 87.3 %–95.1 % in the raw dataset. This reduction in dispersion reflects a more consistent representation of physically plausible conditions following the application of the quality–control procedure, while no clear relationship is observed between PCI and station elevation in the river basins. While the clean PCI is relatively stable, relying on it in isolation can be misleading. Because the PCI represents a relative measure of data consistency, its value depends entirely on the total number of identified snow accumulation events; therefore, highly noisy raw data can produce an artificially high raw PCI, appearing just as reliable as the quality-controlled dataset. An example of this is observed at the Cerro Olivares station (Elqui River Basin), where despite a high Noise Ratio (NR = 2.1) indicating that more than half of the raw SD days were spurious spikes, the raw PCI (90.5 %) is similar to the clean PCI (90.0 %). Complementary, a similar behavior is observed at the Termas del Plomo station (Maipo River Basin), where a higher ΔE value (11) indicates a greater frequency of physically inconsistent accumulation signals, such as rain-to-snow transitions, which are effectively filtered by the algorithm. Despite this substantial removal of inconsistent events, the clean PCI (94.9 %) remains close to the raw PCI (95.1 %), reinforcing that similar PCI values can mask important improvements in the physical consistency of the dataset.

The quality–control procedure evaluation in these stations can be categorized into three groups. The first group comprises stations with higher absolute error removal (ΔE ≥ 2), exhibiting an increase in PCI from 87.3% in the raw data to 94.9% after quality–control procedure. This group includes the Termas del Plomo, Glaciar Juncal Sur, and Glaciar Olivares Alfa stations. The improvement in PCI is associated with the removal of a substantial number of physically inconsistent days (NR ranging from 2 to 11). Notably, NR does not show a direct relationship with the PCI. The second group comprises stations with low error correction (ΔE ≤ 1) and varying proportions of discarded noise (NR ranging from 1.0 to 2.1), which exhibit a slight decrease from raw PCI to quality–control PCI. This behavior is observed at Las Melosas, Glaciar Tapado Corrales in the Elqui River Basin, and Cerro Olivares stations. This marginal decline does not indicate a deterioration in data quality. Rather, the quality–control procedure removes spurious noise, thereby reducing the total sample size (as reflected by NR), which increases the relative influence of the few remaining natural inconsistencies on the final PCI percentage. The third group exhibits a distinct behavior, represented by the Glaciar Olivares Gamma station, which stands out as a unique case of signal recovery. Unlike the previous groups, its metrics explain this pattern: despite no detected errors (ΔE = 0), the quality–control procedure increased the PCI from 89.8% to 94.4%. This improvement did not result from noise filtering, but from the effective correction of data issues associated with sensor mismanagement, which nearly doubled the total number of valid accumulation events (NR = 0.6). Consequently, the few existing natural inconsistencies were mathematically diluted within a much larger sample size, raising the final PCI percentage. Although this station behaves as an outlier, it includes more than 100 analyzed days over six years, enabling this outcome, in contrast to Cerro Olivares, which comprises only 10 analyzed days within a single year of observations.

Table 3. Assessment of snow depth, precipitation, and air temperature data before and after the quality-control procedure in the Elqui and Maipo river basins for the accumulation period May–October, 2017–2024.

Station name	Basin	Latitude (°S)	Elevation (m a.s.l.)	N° days clean overlapped data	Start–End period for clean overlapped data	N° days analyzed for clean data	ΔE	NR	Raw PCI (%)	Clean PCI (%)
Cerro Olivares	Elqui	30.3	3,566	363	2024–2024	10	1	2.1	90.5	90.0
Glaciar Tapado Corrales		30.2	4,065	1,066	2020–2023	28	0	1.2	93.9	92.9
Termas Del Plomo	Maipo	33.6	3,027	1,469	2017–2022	59	11	1.9	87.3	94.9

https://doi.org/10.5194/essd-2026-324
Preprint. Discussion started: 12 May 2026

Las Melosas		33.9	3,317	983	2022–2024	79	1	1.0	95.1	94.9
Glaciar Olivares Gamma		33.2	3,628	1,839	2019–2024	107	0	0.6	89.8	94.4
Glaciar Juncal Sur		33.1	4,035	2,063	2019–2024	110	4	1.4	93.4	94.6
Glaciar Olivares Alfa		33.2	4,230	1,907	2019–2024	72	2	1.4	93.9	94.4

3.4 Deriving snow depth–elevation patterns from *in situ* measurements

Considering the availability of SD observations over the 2010–2024 period, which are characterized by heterogeneous spatial coverage and temporal gaps across elevations and basins, we selected three river basins located in the Arid (Elqui), Mediterranean (Maipo) and Wet Andes (Maule–Itata) that provide relatively consistent SD observations distributed along broad elevation gradients. Despite this selection, none of these basins contain continuous observations for all years and elevations, which limits the analysis of SD variability on a year-by-year basis. To address this limitation, we adopt a representative-year approach based on distinct precipitation conditions, under dry, normal, and wet years (Table A3).

Figure 5 presents the cumulative distribution function (CDF) of SD observations across three river basins, integrating observations during the accumulation period (1 May and 31 October) for each precipitation-year type. This framework enables a robust characterization of the distribution of SD at each station, while the median SD from CDF 0.5 to 1.0 provides a consistent metric for intercomparison across contrasting precipitation-year type and elevations. Across the three basins, a coherent large-scale pattern emerges: SD increases with elevation and from dry to wet years, reflecting the combined control of orographic precipitation and zonal climatic gradients. In dry years, SD distributions are strongly compressed toward low values, considering elevation from 2,000 to 4,500 m a.s.l., with several stations exhibiting less than 50 cm of median SD. In contrast, wet years show a pronounced increase of SD with higher variability of SD over CDF 0.5. This transition is especially marked in the Wet Andes basin (Maule–Itata), where median SD exceeds 200 cm at all stations during wet conditions. Despite this general behavior, the CDF-based analysis indicates that the relationship between SD and elevation is not strictly positive within basins: (i) a positive SD–elevation relationship in the Arid Andes, (ii) a non-positive SD–elevation pattern in the Mediterranean Andes, characterized by mid-elevation SD maxima, and (iii) a consistently high and positive SD–elevation relationship in the Wet Andes.

In the Elqui River Basin (Arid Andes), SD exhibits a strong dependence on elevation and precipitation–year type. During the dry year (2021), median SD values are close to zero at most stations below 3,600 m a.s.l., with only the highest elevation station, Tapado TPF (4,306 m a.s.l.), reaching only 16 cm. Under normal conditions (year 2018), SD increases substantially at high elevations (38 cm at Tapado TPF station), while remaining limited at mid elevations (4 cm at Llano de Liebres station). The wet year (2022) reveals a marked increase of SD across all elevations, considering a similar number of stations and elevation with the dry year, with a clear altitudinal gradient: median SD reaches 132 cm at 4,306 m a.s.l. and remains relatively high (e.g., 55 cm at 3,660 m a.s.l. at El Jote station), although lower elevation stations still exhibit reduced accumulation (< 5 cm at 3,200 m a.s.l. at La Laguna station). These patterns are consistent with a positive SD-elevation relationship.

In the Maipo River Basin (Mediterranean Andes), SD exhibits a complex and spatially heterogeneous distribution along the elevation gradient. During the dry year (2021), median SD remains close to zero at the highest elevations (e.g., Tupungatito Bajo, 4,425 m a.s.l.), while intermediate elevations (3,000–3,400 m a.s.l.) show substantially higher values (e.g. 53 cm at Las Melosas and 27 cm at Termas del Plomo), indicating a non-monotonic SD–elevation relationship. In the normal year (2018), SD increases markedly across a broad elevation range, with several stations between 3,300 and 3,600 m a.s.l. exceeding 100 cm (e.g., Piuquenes14: 102 cm; Las Melosas: 129 cm), whereas lower elevations exhibit reduced values and the highest elevations lack observations. During the wet year (2024), median SD reaches its maximum, particularly at mid elevations (e.g. 260 cm at Las Melosas and 130 cm at Laguna Negra), while remaining comparatively low at elevations above 4,000 m a.s.l. (close to 5 cm at G. Tupungatito Bajo and G. Olivares Alfa). The persistence of this mid-elevation maximum suggests the combined influence of wind-driven snow redistribution and enhanced sublimation at higher elevations, where drier atmospheric conditions could

https://doi.org/10.5194/essd-2026-324
Preprint. Discussion started: 12 May 2026

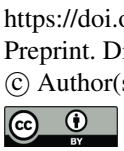

Open Access Earth System Science Data Discussions

limit snow accumulation, thereby preventing the development of a simple positive SD–elevation relationship. Despite the absence of winter-focused studies in this region, Ayala et al. (2017) highlight the significant role of sublimation near 4,500 m a.s.l. on wind-exposed surfaces of the Juncal Norte Glacier.

In the Maule–Itata River Basin (Wet Andes), SD exhibits a more consistent and coherent increase with both elevation and climatic wetness. Even during the dry year (2019), median SD values remain relatively high compared to northern basins (e.g., 77 cm at 1,989 m a.s.l. at Lo Aguirre and 46 cm at 1,977 m a.s.l. at Nevado Longaví). In the normal year (2017), SD increases substantially, reaching 350 cm at 2,439 m a.s.l. (Los Cóndores), with all stations exceeding 50 cm. During the wet year (2024), SD shows a strong amplification across all elevations, with median values exceeding 200 cm at all stations and reaching up to 380 cm at Los Cóndores. Unlike the Elqui and Maipo river basins, the SD–elevation relationship remains largely positive and continuous, reflecting more humid atmospheric conditions and a reduced influence of sublimation at high elevations, which in turn favors more consistent snow accumulation across the elevation gradient in the Wet Andes (Schaefer et al., 2020).

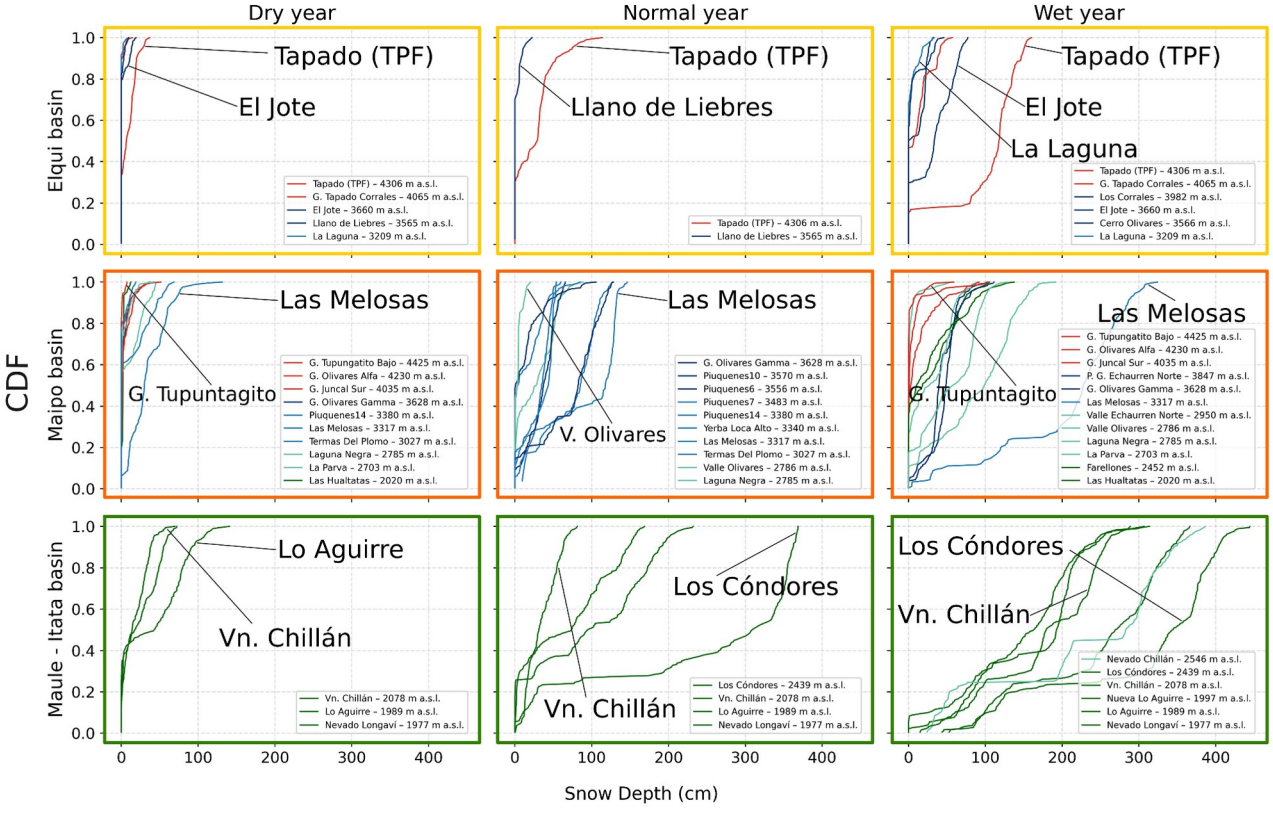

Figure 5. Cumulative distribution functions of snow depth by elevation for specific years with dry, normal, and wet precipitation conditions across three river basins corresponding to each Andean zone. The dry (2021) and normal (2018) years are shared between the Arid and Mediterranean Andes, whereas wet years correspond to 2022 in the Arid Andes and 2024 in the Mediterranean Andes; in contrast, the Wet Andes are represented by a different set of years, with dry (2019), normal (2017), and wet (2004) precipitation conditions. The analysis is based on daily snow depth observations from 1 May to 31 October in the Elqui, Maipo, and Maule–Itata river basins.

https://doi.org/10.5194/essd-2026-324
Preprint. Discussion started: 12 May 2026

Despite the previous analysis based on CDFs under selected dry, normal, and wet precipitation conditions, a more robust assessment of SD observations is undertaken by examining the SD–elevation relationship in conjunction with the hypsometry of each of the three river basins.

Figure 6A, shows how SD increases consistently with the rise in total precipitation from the arid to the wet zones of Chile, as expected (Sarricolea et al., 2017). Furthermore, we observed the same SD-elevation pattern analysed through CDF in the three river basins. In the Elqui River Basin (29° S), a positive relationship between SD and elevation is observed for the dry (2021) and normal (2018) precipitation types, although in the wet year (2022) this pattern is interrupted: SD increases up to approximately 3,600 m a.s.l., then declines toward 4,000 m a.s.l., before increasing again up to the highest elevations with available SD observations (4,300 m a.s.l.). These features are reflected in the 25th and 75th percentile SD observations. In the Maipo River Basin (33° S), the SD–elevation relationship remains positive up to approximately 2,800–3,300 m a.s.l. across all climate types. Available data further suggest that above 3,300 m a.s.l., SD begins to decline. In contrast, SD observations in the Maule–Itata River Basin (37° S) exhibit a consistently positive SD–elevation relationship.

Although such SD–elevation patterns have not been previously documented in Chile at the basin scale over a wide elevation range, existing studies restricted to small microcatchments in Maipo River Basin with short observational periods provide only partial insights. Mendoza et al. (2020) examined microcatchments in the Arid and Mediterranean Andes within a relatively narrow elevation range, finding that SD increased between 3,600 and 3,900 m a.s.l. In 2018, followed by a decrease at higher elevations, and that SD values declined on slopes steeper than 35°. Similarly, Shaw et al. (2020a,b) showed in a microcatchment of the Mediterranean Andes that SWE increased from approximately 3,000 to 3,800 m a.s.l., then declined up 5,400 m a.s.l., in the period 2017–2018.

The elevational distribution of SD stations under these precipitation regimes supports the observed SD patterns across the three river basins. Figure 6B presents the distribution of SD stations by elevation alongside the hypsometric curve for each basin. The lower bound of the hypsometric curve represents the minimum elevation of July snow persistence over the 2000–2024 period, while the elevation corresponding to the 25th percentile of snow persistence is indicated by a thick line.

Despite the generally well-distributed elevation range of stations, the Elqui River Basin includes five SD stations that do not provide observations during normal precipitation years, highlighting the critical role of CEAZA stations in characterizing the SD–elevation relationship in this basin. A comparable spatial distribution of SD stations across the three precipitation regimes is observed in the Maipo River Basin; however, of the 18 stations, nine do not capture normal years, particularly at the lowest and highest elevations. Although the SD network is largely composed of DGA stations, 13 spanning a broad elevation range (2,020–4,230 m a.s.l.), stations operated by UdeChile provide important complementary coverage in the Mapocho sub-basin. In contrast, the Maule–Itata River Basin is entirely dominated by DGA stations, where three stations lack data for dry precipitation years.

As a result, when considering only these three specific precipitation conditions, just six stations capture SD variability across the Maule–Itata River Basin, which encompasses a snow-covered area of 30,690 km² as defined by the snow line elevation estimated here. This contrasts with the smaller snow-covered areas of the Elqui (6,460 km²) and Maipo (7,730 km²) river basins, where a denser SD station network is available.

https://doi.org/10.5194/essd-2026-324
Preprint. Discussion started: 12 May 2026

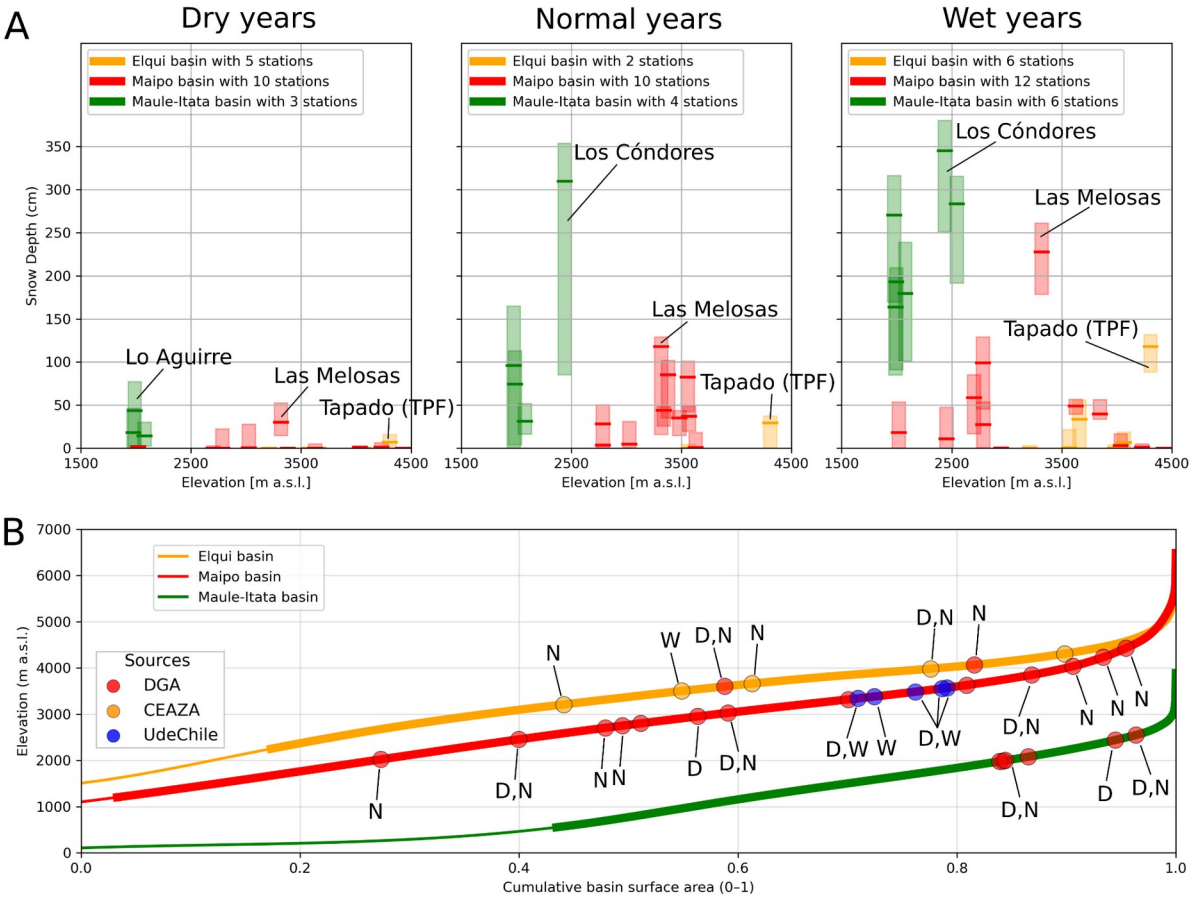

Figure 6. Measured relationships between snow depth and elevation for three precipitation–year types, dry (D), normal (N), and wet (W), across three river basins representing the Arid (Elqui, 29° S), Mediterranean (Maipo, 33° S), and Wet (Maule–Itata, 37° S) Andes in Chile. Only if present SD observations from stations with at least 70 % of daily observations per month during the accumulation period (1 May to 31 October). In each upper panel (A), bars represent the 25th, 50th, and 75th percentile SD values, derived from all available observations for the selected precipitation years. The lower panel (B) compares station elevations with the basin hypsometric curves. The thin line indicates the minimum elevation of July snow persistence over the 2000–2024 period, while the thick line marks the elevation at which snow persistence reaches the 25th percentile (SP25). Circles denote the elevation of SD stations and are labeled according to the lagged precipitation year type (D, N, or W). Stations without labels correspond to sites with SD observations available under all three precipitation years.

4 Data availability

The dataset is openly available via Zenodo at https://doi.org/10.5281/zenodo.20089265 (Medina and Caro, 2026). An interactive snow depth exploration tool is also provided at https://javiermedinamen-art.github.io/hidromet, developed by the Observatorio Satelital de Nieves laboratory.

Input data were obtained from publicly accessible repositories and institutional collaborations, including the DGA, CEAZA (or CEAZAMET), IANIGLA, University of Chile, and CIEP. DGA data are distributed through the Chilean open-data framework,

https://doi.org/10.5194/essd-2026-324
Preprint. Discussion started: 12 May 2026

which allows data reuse and redistribution with proper attribution. CEAZA data usage policies explicitly allow their use in scientific publications with acknowledgment of the original source. Datasets from IANIGLA, University of Chile, and CIEP were provided directly by these institutions for scientific research purposes, and co-authors actively affiliated with these institutions facilitated access to the corresponding datasets. The original observations were reprocessed and integrated into the derived dataset distributed in this study while maintaining attribution to the original data providers.

5 Code availability

A short code to run the quality–control procedure is available via Github at https://github.com/javiermedinamen-art/hidromet/tree/main/sd_cleaning_sample, applied to the Valle Olivares station (33° S).

6 Conclusions

This open–access, quality–controlled snow depth dataset represents the largest and most complete collection of continuous snow depth data for the Southern Andes. Of the 118 continuous snow depth measurement stations across Chile and Argentina, 81 were selected for inclusion in the final consistent and quality-controlled daily dataset, providing records between 21° and 54° S. This dataset offers unprecedented spatial and elevational coverage across the Southern Andes, integrating over fifteen years of observations (2010–2024). The quality–control procedure improved data reliability, increasing the newly proposed Physical Consistency Index from 90.5 % in the raw dataset to 92.9 % in the quality–controlled dataset for stations in the Elqui River Basin, and from 87.3 % to 94.9 % for stations in the Maipo River Basin. These improvements demonstrate the effectiveness of the quality–control procedure, even when the volume of data finally available is significantly reduced. This improvement enables us to distinguish river basins with high and low station completeness, and to identify where the snow depth–elevation relationship can be reliably characterized. The main conclusions are as follows.

- No clear latitudinal pattern is observed in station data quality across the 26 river basins. Instead, data quality limitations are more pronounced in basins located in the Wet Andes, where the proportion of high-quality stations is generally lower and the total number of stations is also limited. This is the case for the Valdivia (two stations), Biobío (five stations), and Baker and Costeras e Islas R. Aisén–R. Baker basins (three stations), which exhibit the largest reductions in data availability (>50 %) after quality control. In contrast, basins with a single station tend to retain most of their observations (>99 %), as observed in the Yelcho, Bueno, and Tunuyán river basins, although their representativeness remains limited. Notably, the Elqui and Maipo river basins, which have the highest station densities (7 and 21 stations, respectively), show only minor reductions after quality control, indicating a higher proportion of high-quality observations and strong potential for robust snow depth analyses.

- Despite the availability of 81 snow depth stations in our final quality-controlled daily SD dataset, only three river basins provide sufficient elevational coverage to characterize basin-scale snow depth–elevation patterns across the Andean zones. Two of these basins exhibit non–linear relationships, with maximum snow accumulation occurring at approximately 3,300 m a.s.l. in the Maipo River Basin (Mediterranean Andes) and 4,300 m a.s.l. in the Elqui River Basin (Arid Andes). In contrast, a linear SD–elevation relationship is identified in the Maule–Itata River Basin (Wet Andes); however, this result likely reflects limitations in elevational representativeness due to the limited elevation range of the available stations.

https://doi.org/10.5194/essd-2026-324
Preprint. Discussion started: 12 May 2026

- The distribution of SD monitoring stations does not reflect the relative spatial extent of snow-covered areas in the study domain. The Maule–Itata River Basin has the largest snow-covered area (30,690 km²) yet a comparatively lower station density than the smaller Elqui (6,460 km²) and Maipo (7,730 km²) river basins. In both the Maule–Itata and Elqui river basins, the DGA network is strongly complemented by stations operated by Universidad de Chile and CEAZA, which are essential for improving the characterization of SD–elevation patterns.

Finally, the resulting snow depth dataset offers new opportunities to advance research on snow-related hydrological processes across one of the most diverse mountain systems in the Southern Hemisphere. At the same time, it underscores the need to improve the data availability and spatial representativeness of *in situ* snow depth observations, which must be prioritized through informed policy decisions, with scientific capacity serving as a key support to improve the quality of snow depth observations.

Author contributions

AC conceived the study and defined its scope. AC and JM compiled the station dataset, designed the quality–control procedure, performed the analyses, and prepared the tables and figures. JM developed the quality–control algorithm. AC drafted the first version of the manuscript. All co-authors reviewed and revised the manuscript.

Competing interests

The contact author has declared that none of the authors has any competing interests.

Acknowledgements

The authors gratefully acknowledge DGA, CEAZA, the Department of Civil Engineering at the University of Chile, Marlene Huerta, CIEP, CECS, and IANIGLA for providing the snow depth data used in this study. This research was supported by the Agencia Nacional de Investigación y Desarrollo de Chile (ANID) through the FONDEF project IT24I0092 (2024–2026). We also thank the reviewers for their constructive comments, which helped to improve the quality of this article.

Financial support

This article was supported by the FONDEF IT IT24I0092 project 2024–2026.

References

Aguayo R., León-Muñoz J., Aguayo M., Baez-Villanueva O., Fernandez A., Zambrano-Bigiarini M., et al.: PatagoniaMet: A multi-source hydrometeorological dataset for Western Patagonia. Sci. Data. 11, 6, 10.1038/s41597-023-02828-2, 2024.

Alvarez-Garreton, C., Boisier, J. P., Garreaud, R., Seibert, J., and Vis, M.: Progressive water deficits during multiyear droughts in basins with long hydrological memory in Chile, Hydrol. Earth Syst. Sci., 25, 429–446, doi:10.5194/hess-25-429-2021, 2021.

Ayala, Á., Pellicciotti, F., Peleg, N., and Burlando, P.: Melt and surface sublimation across a glacier in a dry environment: distributed energy-balance modelling of Juncal Norte Glacier, Chile, J. Glaciol., 63, 803–822, doi:10.1017/jog.2017.46, 2017.

Ayala, Á., Farías-Barahona, D., Huss, M., Pellicciotti, F., McPhee, J., and Farinotti, D.: Glacier runoff variations since 1955 in the Maipo River basin, in the semiarid Andes of central Chile, Cryosphere, 14, 2005–2027, doi:10.5194/tc-14-2005-2020, 2020.

Ayala, Á., Muñoz-Castro, E., Farinotti, D. et al.: Less water from glaciers during future megadroughts in the Southern Andes, Commun Earth Environ 6, 860, doi:10.1038/s43247-025-02845-6, 2025.

Bulovic, N., Johnson, F., Lievens, H., Shaw, T. E., McPhee, J., Gascoin, S., Demuzere, M., and McIntyre, N.: Evaluating the performance of Sentinel-1 SAR derived snow depth retrievals over the extratropical Andes Cordillera, Water Resour. Res., 61, e2024WR037766, doi:10.1029/2024WR037766, 2025.

Burger, F., Ayala, Á., Farías, D., Shaw, T. E., MacDonell, S., Brock, B., McPhee, J., and Pellicciotti, F.: Interannual variability in glacier contribution to runoff from a high-elevation Andean catchment: Understanding the role of debris cover in glacier hydrology, Hydrol. Process., 33, 214–229, doi:10.1002/hyp.13354, 2019.

Caro, A., Condom, T., and Rabatel, A.: Climatic and morphometric explanatory variables of glacier changes in the Andes (8–55° S): New insights from machine learning approaches, Front. Earth Sci., 9, 713011, doi:10.3389/feart.2021.713011, 2021.

Caro, A., Condom, T., Rabatel, A., Champollion, N., García, N., and Saavedra, F.: Hydrological response of Andean catchments to recent glacier mass loss, Cryosphere, 18, 2487–2507, doi:10.5194/tc-18-2487-2024, 2024.

Caro, A., Condom, T., Rabatel, A. et al.: Future glacio-hydrological changes in the Andes: a focus on near-future projections up to 2050, Sci Rep 15, 10991, doi:10.1038/s41598-025-88069-2, 2025

Cornwell, E., Molotch, N. P., and McPhee, J.: Spatio-temporal variability of snow water equivalent in the extra-tropical Andes Cordillera from distributed energy balance modeling and remotely sensed snow cover, Hydrol. Earth Syst. Sci., 20, 411–430, doi:10.5194/hess-20-411-2016, 2016.

Cortés, G. and Margulis, S.: Impacts of El Niño and La Niña on interannual snow accumulation in the Andes: Results from a high-resolution 31-year reanalysis, Geophys. Res. Lett., 44, 6859–6867, doi:10.1002/2017GL073826, 2017.

https://doi.org/10.5194/essd-2026-324
Preprint. Discussion started: 12 May 2026

Durre, I., Menne, M. J., Gleason, B. E., Houston, T. G., and Vose, R. S.: Comprehensive automated quality assurance of daily surface observations, J. Appl. Meteorol. Clim., 49, 1615–1633, doi:10.1175/2010JAMC2375.1, 2010.

Dussaillant, A., Buytaert, W., Meier, C., and Espinoza, F.: Hydrological regime of remote catchments with extreme gradients under accelerated change: the Baker basin in Patagonia, Hydrolog. Sci. J., 57, 1530–1542, doi:10.1080/02626667.2012.726993, 2012.

Garreaud, R. D., Alvarez-Garreton, C., Barichivich, J., Boisier, J. P., Christie, D., Galleguillos, M., LeQuesne, C., McPhee, J., and Zambrano-Bigiarini, M.: The 2010–2015 megadrought in central Chile: Impacts on regional hydroclimate and vegetation, Hydrol. Earth Syst. Sci., 21, 6307–6327, doi:10.5194/hess-21-6307-2017, 2017.

Garreaud, R. D., Boisier, J. P., Rondanelli, R., Montecinos, A., Sepúlveda, H. H., and Veloso-Aguila, D.: The central Chile mega drought (2010–2018): A climate dynamics perspective, Int. J. Climatol., 40, 421–439, doi:10.1002/joc.6219, 2020.

Garreaud, R., Boisier, J. P., Alvarez-Garreton, C., Christie, D. A., Carrasco-Escaff, T., Vergara, I., Chávez, R. O., Aldunce, P., Camus, P., Suazo-Álvarez, M., Masiokas, M., Castro, G., Muñoz, A., Zambrano-Bigiarini, M., Fuster, R., and Godoy, L.: Hyperdroughts in central Chile: drivers, impacts, and projections, Hydrol. Earth Syst. Sci., 29, 5347–5369, doi:10.5194/hess-29-5347-2025, 2025.

Grünewald, T., Bühler, Y., and Lehning, M.: Elevation dependency of mountain snow depth, Cryosphere, 8, 2381–2394, doi:10.5194/tc-8-2381-2014, 2014.

Huerta, M.L., Molotch N.P., McPhee J.: Snowfall interception in a deciduous Nothofagus forest and implications for spatial snowpack distribution, Hydrological Processes, 33, 1818–1834, doi:10.1002/hyp.13439, 2019.

Instituto Nacional de Estadísticas (INE): Resultados Censo 2024, available at: https://censo2024.ine.gob.cl/resultados/ (last access: 10 December 2025), 2024.

Instituto Nacional de Estadísticas (INE): Gráficas nacionales – Resultados del VIII Censo Nacional Agropecuario y Forestal, available at: https://www.ine.gob.cl/censoagropecuario/resultados-finales/graficas-nacionales (last access: 10 December 2025), 2022.

Krogh, S. A., Pomeroy, J. W., and McPhee, J.: Physically based mountain hydrological modeling using reanalysis data in Patagonia, J. Hydrometeorol., 16, 172–193, doi:10.1175/JHM-D-13-0178.1, 2015.

MacDonell, S., Kinnard, C., Mölg, T., Nicholson, L., and Abermann, J.: Meteorological drivers of ablation processes on a cold glacier in the semi-arid Andes of Chile, Cryosphere, 7, 1513–1526, doi:10.5194/tc-7-1513-2013, 2013.

Masiokas, M. H., Rabatel, A., Rivera, A., Ruiz, L., Pitte, P., Ceballos, J. L., Barcaza, G., Soruco, A., Bown, F., Berthier, E., Dussaillant, I., and MacDonell, S.: A review of the current state and recent changes of the Andean cryosphere, Front. Earth Sci., 8, 99, doi:10.3389/feart.2020.00099, 2020.

Masiokas, M. H., Cara, L., Villalba, R., Pitte, P., Luckman, B. H., Toum, E., Christie, D. A., Le Quesne, C., and Mauget, S.: Streamflow variations across the Andes (18°–55°S) during the instrumental era, Sci Rep, 9, 17879, doi:10.1038/s41598-019-53981-x, 2019.

Masiokas, M. H., Christie, D. A., Le Quesne, C., Pitte, P., Ruiz, L., Villalba, R., Luckman, B. H., Berthier, E., Nussbaumer, S. U., González-Reyes, Á., McPhee, J., and Barcaza, G.: Reconstructing the annual mass balance of the Echaurren Norte glacier (Central Andes, 33.5° S) using local and regional hydroclimatic data, The Cryosphere, 10, 927–940, doi.org/10.5194/tc-10-927-2016, 2016.

Medina, J., and Caro, A.: The Southern Andes Daily Snow Depth Dataset (2010–2024): quality-controlled dataset from Chile and Argentina, Zenodo [data set], https://doi.org/10.5281/zenodo.20089265, 2026.

Mendoza, P. A., Shaw, T. E., McPhee, J., Musselman, K. N., Revuelto, J., & MacDonell, S.: Spatial distribution and scaling properties of lidar-derived snow depth in the extratropical Andes. Water Resources Research, 56, e2020WR028480, doi.org/10.1029/2020WR028480, 2020.

Ntokas, K. F. F., Odry, J., Boucher, M. A., and Garnaud, C.: Investigating ANN architectures and training to estimate snow water equivalent from snow depth, Hydrol. Earth Syst. Sci., 25, 3017–3040, doi:10.5194/hess-25-3017-2021, 2021.

Pandas development team: pandas-dev/pandas: Pandas (version 2.3.0), Zenodo, doi:10.5281/zenodo.15597513, 2025.

Perkins, R. M. and Jones, J. A.: Climate variability, snow, and physiographic controls on storm hydrographs in small forested basins, western Cascades, Oregon, Hydrol. Process., 22, 4949–4964, doi:10.1002/hyp.7117, 2008.

Rivera, D., Godoy-Faúndez, A., Lillo, M., Alvez, A., Delgado, V., Gonzalo-Martín, C., Menasalvas, E., Costumero, R., and García-Pedrero, Á.: Legal disputes as a proxy for regional conflicts over water rights in Chile, Journal of Hydrology, 535, 36–45, https://doi.org/10.1016/j.jhydrol.2016.01.057, 2016.

Rousseeuw, P. J., & Croux, C.: Alternatives to the Median Absolute Deviation. Journal of the American Statistical Association, 88(424), 1273–1283, doi.org/10.1080/01621459.1993.10476408, 1993.

Saavedra, F. A., Kampf, S. K., Fassnacht, S. R., and Sibold, J. S.: A snow climatology of the Andes Mountains from MODIS snow cover data, Int. J. Climatol., 37, 1526–1539, doi:10.1002/joc.4795, 2017.

Saavedra, F. A., Kampf, S. K., Fassnacht, S. R., and Sibold, J. S.: Changes in Andes snow cover from MODIS data, 2000–2016, The Cryosphere, 12, 1027–1046, doi.org/10.5194/tc-12-1027-2018, 2018.

Saavedra et al., Spatial and Temporal Variability of Snow in the Andes using MODIS Snow Product 2000-2024, Front. Earth Sci., 2026, https://www.frontiersin.org/journals/earth-science/articles/10.3389/feart.2026.1564035/abstract

Sarricolea, P., Herrera-Ossandon, M., and Meseguer-Ruiz, Ó.: Climatic regionalisation of continental Chile, J. Maps, 13, 66–73, doi:10.1080/17445647.2016.1259592, 2017.

Scaff, L., Rutllant, J. A., Rahn, D., Gascoin, S., and Rondanelli, R.: Meteorological interpretation of orographic precipitation gradients along an andes west slope basin at 30° S (Elqui valley, Chile). J. Hydrometeorol. 18 (3), 713–727, doi:10.1175/JHM-D-16-0073.1, 2017.

Schaefer, M., Fonseca-Gallardo, D., Farías-Barahona, D., and Casassa, G.: Surface energy fluxes on Chilean glaciers: measurements and models, The Cryosphere, 14, 2545–2565, doi:10.5194/tc-14-2545-2020, 2020.

Servicio Nacional de Geología y Minería (SERNAGEOMIN). Anuario de la Minería de Chile (Tech. Rep.). Servicio Nacional de Geología y Minería, 2021.

Shaw, T. E., Caro, A., Mendoza, P., Ayala, Á., Pellicciotti, F., Gascoin, S., and McPhee, J.: The utility of optical satellite winter snow depths for initializing a glacio-hydrological model of a high-elevation Andean catchment, Water Resour. Res., 56, e2020WR027188, doi:10.1029/2020WR027188, 2020a.

https://doi.org/10.5194/essd-2026-324
Preprint. Discussion started: 12 May 2026

771 Shaw, T. E., Gascoin, S., Mendoza, P. A., Pellicciotti, F., and McPhee, J.: Snow Depth Patterns in a High Mountain Andean
772 Catchment from Satellite Optical Tristereoscopic Remote Sensing, Water Resour. Res., 56, e2019WR024880,
773 doi.org/10.1029/2019wr024880, 2020b.
774
775 Stewart, I. T.: Changes in snowpack and snowmelt runoff for key mountain regions, Hydrological Processes, 23, 78–94,
776 doi:10.1002/hyp.7128, 2009.
777
778 Viale, M. and Nuñez, M. N.: Climatology of Winter Orographic Precipitation over the Subtropical Central Andes and
779 Associated Synoptic and Regional Characteristics, J. Hydrometeorol., 12, 481–507, doi.org/10.1175/2010JHM1284.1, 2011.
780
781 Voordendag, A., Réveillet, M., MacDonell, S., and Lhermitte, S.: Snow model comparison to simulate snow depth evolution
782 and sublimation at point scale in the semi-arid Andes of Chile, Cryosphere, 15, 4241–4259, doi:10.5194/tc-15-4241-2021,
783 2021.

784 **Appendix**

Table A1. Characteristics of 81 selected stations with snow depth observations in Chile and Argentina across 21–54° S

Name	Latitude (°)	Longitude (°)	Elevation (m a.s.l.)	Basin	Source	Code	Snow depth sensor
Volcán Auncanquilcha	-21.1906	-68.4528	5,087	Fronterizas Salar Michincha	DGA	02000002	Campbell/SR50A was replaced by Lufft/SHM31
Cerro Chajnantor Cumbre	-22.9872	-67.7422	5,625	Endorreica entre Front. y S. Atacama	DGA	02400002	Campbell/SR50A was replaced by Lufft/SHM31
Volcán Ojos del Salado bajo Refugio Atacama	-27.0519	-68.5350	5,201	Endorreicas entre Front. y Vertiente	DGA	03031002	Campbell/SR50A was replaced by Lufft/SHM31
Volcán Ojos del Salado en Refugio Tejos	-27.0869	-68.5378	5,804	Endorreicas entre Front. y Vertiente	DGA	03031003	Campbell/SR50A was replaced by Lufft/SHM31
Glaciar Maranceles	-28.4572	-69.7236	3,985	Río Copiapo	DGA	03413001	Campbell/SR50A was replaced by Lufft/SHM31
Glaciar Tapado en Los Corrales	-30.1554	-69.8829	4,065	Río Elqui	DGA	04300004	Campbell/SR50A was replaced by Lufft/SHM31
Tapado (TPF)	-30.1584	-69.9084	4,306	Río Elqui	CEAZA	0430004	Lufft/SHM31
Los Corrales	-30.1615	-69.8759	3,982	Río Elqui	CEAZA	0430014	Campbell/SR50A
Capayán	-30.1734	-69.8038	4,754	Río Jáchal	IANIGLA	Capayán	Campbell/SR50A
La Laguna	-30.2032	-70.0371	3,209	Río Elqui	CEAZA	0430009	Campbell/SR50A
Llano de Las Liebres	-30.2542	-69.9345	3,565	Río Elqui	CEAZA	0430012	Campbell/SR50A

https://doi.org/10.5194/essd-2026-324
Preprint. Discussion started: 12 May 2026

Cerro Olivares	-30.2567	-69.9355	3,566	Río Elqui	DGA	04300001	Campbell/SR50A was replaced by Lufft/SHM31
El Jote	-30.4053	-70.2795	3,660	Río Elqui	CEAZA	0430003	Campbell/SR50A
Quebrada Larga Cota 3500	-30.7252	-70.2918	3,550	Río Limarí	DGA	04520006	Campbell/SR50A was replaced by Lufft/SHM31
Cerro Vega Negra	-30.9059	-70.5165	3,529	Río Limarí	DGA	04511004	Campbell/SR50A was replaced by Lufft/SHM31
Tascadero	-31.2628	-70.5399	3,427	Río Limarí	CEAZA	0450001	Campbell/SR50A
Casa del Canto	-31.4173	-70.5890	3,570	Río Choapa	CEAZA	0470001	Campbell/SR50A
El Soldado	-32.0066	-70.3213	3,293	Río Choapa	DGA	04700002	Campbell/SR50A was replaced by Lufft/SHM31
Nacimiento Del Sobrante	-32.1889	-70.4829	3,143	Río Petorca	DGA	05100003	Campbell/SR50A was replaced by Lufft/SHM31
Las Cuevas	-32.8130	-70.0530	3,197	Río Mendoza	IANIGLA	Cuevas	Campbell/SR50A
Portillo	-32.8424	-70.0970	3,032	Río Aconcagua	DGA	05401007	Campbell/SR50A was replaced by Lufft/SHM31
Glaciar León Negro	-32.9936	-70.0283	4,350	Río Aconcagua	DGA	05400005	Campbell/SR50A was replaced by Lufft/SHM31
Portillo Argentino	-33.6219	-69.6078	4.,336	Río Mendoza	IANIGLA	Portillo	Campbell/SR50A
Glaciar Juncal Sur	-33.1175	-70.1119	4,035	Río Maipo	DGA	05706004	Campbell/SR50A was replaced by Lufft/SHM31
Glaciar Olivares Gamma	-33.1564	-70.1528	3,628	Río Maipo	DGA	05706002	Campbell/SR50A was replaced by Lufft/SHM31
Glaciar Olivares Alfa	-33.1786	-70.2181	4,230	Río Maipo	DGA	05706005	Campbell/SR50A was replaced by Lufft/SHM31
Valle Olivares	-33.1910	-70.1141	2,786	Río Maipo	DGA	05706003	Campbell/SR50A was replaced by Lufft/SHM31
Yerba Loca Alto	-33.2092	-70.2769	3,340	Río Maipo	UdeChile	AMTC10	Campbell/SR50A
Yerba Loca Medio	-33.2730	-70.3000	2,520	Río Maipo	UdeChile	AMTC8	Campbell/SR50A
Molina en Cepo	-33.2910	-70.2173	3,380	Río Maipo	UdeChile	AMTC13	Campbell/SR50A
Piuquenes 10	-33.3126	-70.2481	3,570	Río Maipo	UdeChile	Piuquenes 10	MaxBotix/MB7389 HRXL-MaxSonar-WRMT
Piuquenes 7	-33.3133	-70.2561	3,483	Río Maipo	UdeChile	Piuquenes 7	MaxBotix/MB7389 HRXL-MaxSonar-WRMT
Piuquenes 6	-33.3165	-70.2611	3,556	Río Maipo	UdeChile	Piuquenes 6	MaxBotix/MB7389 HRXL-MaxSonar-WRMT
Piuquenes 14	-33.3176	-70.2516	3,380	Río Maipo	UdeChile	Piuquenes 14	MaxBotix/MB7389 HRXL-MaxSonar-WRMT
La Parva	-33.3306	-70.2972	2,703	Río Maipo	DGA	05721019	Campbell/SR50A was replaced by Lufft/SHM31
Farellones	-33.3517	-70.3128	2,452	Río Maipo	DGA	05720005	Campbell/SR50A was replaced by Lufft/SHM31
Molina Medio	-33.3753	-70.2413	2,200	Río Maipo	UdeChile	AMTC12	Campbell/SR50A
Glaciar	-33.3858	-69.8381	4,425	Río Maipo	DGA	05705004	Campbell/SR50A was

https://doi.org/10.5194/essd-2026-324
Preprint. Discussion started: 12 May 2026

Tupungatito Bajo							replaced by Lufft/SHM31
Portezuelo Glaciar Echaurren Norte	-33.5764	-70.1289	3,847	Río Maipo	DGA	05703013	Campbell/SR50A was replaced by Lufft/SHM31
Valle Echaurren Norte	-33.5939	-70.1103	2,950	Río Maipo	DGA	05703012	Campbell/SR50A was replaced by Lufft/SHM31
Termas Del Plomo	-33.6133	-69.9058	3,027	Río Maipo	DGA	05703014	Campbell/SR50A was replaced by Lufft/SHM31
Laguna Negra	-33.6659	-70.1077	2,785	Río Maipo	DGA	05703009	Campbell/SR50A was replaced by Lufft/SHM31
Las Melosas Ruta de Nieve	-33.8636	-70.2727	3,317	Río Maipo	DGA	05701010	Campbell/SR50A was replaced by Lufft/SHM31
Las Hualtatas	-34.0677	-70.1089	2,020	Río Maipo	DGA	05701011	Campbell/SR50A was replaced by Lufft/SHM31
Codelco Cerro Teniente	-34.2047	-70.2692	2,950	Río Rapel	DGA	06005005	Campbell/SR50A was replaced by Lufft/SHM31
Laguna El Yeso	-34.4118	-70.2084	2,140	Río Rapel	DGA	06000004	Campbell/SR50A was replaced by Lufft/SHM31
Laguna Los Cristales	-34.5611	-70.5097	2,357	Río Rapel	DGA	06013008	Campbell/SR50A was replaced by Lufft/SHM31
Glaciar Cortaderal	-34.6608	-70.2561	3,156	Río Rapel	DGA	06001000	Campbell/SR50A was replaced by Lufft/SHM31
Glaciar Universidad en Río San Andrés	-34.7186	-70.3592	2,436	Río Rapel	DGA	06023000	Campbell/SR50A was replaced by Lufft/SHM31
Cerro Los Guzmanes	-34.8861	-70.4636	3,125	Río Rapel	DGA	06021002	Campbell/SR50A was replaced by Lufft/SHM31
Termas Del Flaco	-34.8930	-70.3300	2,665	Río Rapel	DGA	06020001	Campbell/SR50A was replaced by Lufft/SHM31
Paso Vergara	-35.1948	-70.5114	2,602	Río Mataquito	DGA	07100006	Campbell/SR50A was replaced by Lufft/SHM31
Toqui Lautaro	-35.2928	-70.5163	2,453	Río Tunuyán	IANIGLA	Toqui	Campbell/SR50A
Lo Aguirre	-35.9713	-70.5721	1,989	Río Maule	DGA	07301000	Campbell/SR50A was replaced by Lufft/SHM31
NUEVA LO AGUIRRE	-35.9723	-70.5718	1,997	Río Maule	DGA	07301002	Campbell/SR50A was replaced by Lufft/SHM31
Los Condores	-36.0097	-70.5478	2,439	Río Maule	DGA	07301001	Campbell/SR50A was replaced by Lufft/SHM31
Nevado Longavi	-36.2344	-71.1435	1,977	Río Maule	DGA	07350008	Campbell/SR50A was replaced by Lufft/SHM31
Nevado Chillan	-36.8473	-71.4160	2,546	Río Itata	DGA	08130009	Campbell/SR50A was replaced by Lufft/SHM31
Volcan Chillan	-36.8939	-71.4116	2,078	Río Biobio	DGA	08374001	Campbell/SR50A was replaced by Lufft/SHM31
Node3	-36.9103	-71.3989	1,938	Río Itata	UdeChile	081003	Campbell/SR50A
Node2	-36.9104	-71.4089	1,809	Río Itata	UdeChile	081002	Campbell/SR50A

https://doi.org/10.5194/essd-2026-324
Preprint. Discussion started: 12 May 2026

Open Access Earth System Science Data Discussions

Node1	-36.9148	-71.4166	1,633	Río Itata	UdeChile	081001	Campbell/SR50A
Node4	-36.9205	-71.4180	1,695	Río Itata	UdeChile	081004	Campbell/SR50A
Alto Mallines	-37.1578	-71.2430	1,784	Río Biobio	DGA	08372001	Campbell/SR50A was replaced by Lufft/SHM31
Los Corralitos	-37.5772	-71.1575	1,785	Río Biobio	DGA	08370010	Campbell/SR50A was replaced by Lufft/SHM31
Chenqueco	-38.0647	-71.3547	778	Río Biobio	DGA	08308003	Campbell/SR50A was replaced by Lufft/SHM31
Liucura	-38.6449	-71.0907	1,034	Río Biobio	DGA	08301001	Campbell/SR50A was replaced by Lufft/SHM31
Volcán Villarrica Pichillancahue	-39.4350	-71.8758	1,800	Río Valdivia	DGA	10105003	Campbell/SR50A was replaced by Lufft/SHM31
Complejo Volcánico Mocho Choshuenco	-39.9514	-72.0586	1,565	Río Valdivia	DGA	10110003	Campbell/SR50A was replaced by Lufft/SHM31
Cardenal Samore	-40.6831	-71.9864	920	Río Bueno	DGA	10321001	Campbell/SR50A was replaced by Lufft/SHM31
Cuesta Moraga	-43.3360	-72.3990	575	Río Yelcho	DGA	10710004	Campbell/SR50A was replaced by Lufft/SHM31
Cerro Divisadero	-45.6165	-72.0134	1,430	Río Aysén	CIEP	1130001	Campbell/SR50A
Cerro Divisadero en el Fraile	-45.6270	-72.0040	1,190	Río Aysén	DGA	11314002	Campbell/SR50A was replaced by Lufft/SHM31
Portezuelo Ibañez	-46.0778	-72.0510	1,080	Río Baker	DGA	11503002	Campbell/SR50A was replaced by Lufft/SHM31
Hielo Norte en Glaciar San Rafael	-46.7053	-73.5936	1,187	Cost. e Islas R. Aisén R. Baker	DGA	11440001	Campbell/SR50A was replaced by Lufft/SHM31
Steffen	-47.5555	-73.6958	30	Río Baker	CIEP	1150003	Campbell/SR50A
Epulef	-49.0523	-72.9505	898	Río Santa Cruz	IANIGLA	Epulef	Campbell/SR50A
Aonikenk	-49.2774	-72.9975	1,233	Río Santa Cruz	IANIGLA	Aonikenk	Campbell/SR50A
Chalten	-49.3381	-72.8844	400	Río Santa Cruz	IANIGLA	Chalten	Campbell/SR50A
Pliegue Tumbado	-49.3793	-72.9368	1,070	Río Santa Cruz	IANIGLA	Tumbado	Campbell/SR50A
Glaciar Snoring	-53.7230	-72.6080	70	Islas al sur Est. de Magallanes	DGA	12730001	Campbell/SR50A was replaced by Lufft/SHM31

https://doi.org/10.5194/essd-2026-324
Preprint. Discussion started: 12 May 2026

Open Access Earth System Science Data Discussions

Table A2. Characteristics of 37 excluded stations with snow depth observations in Chile and Argentina across 17–55° S.

Name	Lat (°)	Long (°)	Elevation (m a.s.l.)	Basin	Source	Issue
Volcán Tacora	-17.6940	-69.7730	5,047	Río Lluta Alto	DGA	Poor data quality from 2022 to 2025
Volcán Quimsachata	-19.7510	-68.7870	5,076	Quebrada de Tarapacá	DGA	Poor data quality in 2022
Paso Jama	-22.9220	-67.7010	4,680	Salar de Atacama	DGA	Poor data quality in 2025

786

https://doi.org/10.5194/essd-2026-324
Preprint. Discussion started: 12 May 2026

787

Toconao Pueblo	-23.1861	-68.0056	2,491	Salar de Atacama	DGA	Poor data quality from 2017 to 2026; no ground reference height
Paso Sico	-23.8225	-67.4388	4,295	Salar de Atacama	DGA	Poor data quality between 2017 and 2026
Volcán LLullaillaco	-24.6760	-68.5700	4,800	Endorreicas Salar Atacama-Vertiente Pacifico	DGA	Data since 2026
El Tapado 2	-30.1540	-69.8960	4,250	Río Elqui	CEAZA	Poor data quality
Cuesta Blanca	-31.0970	-70.4170	3,284	Río Limari	DGA	Data available only during summer 2025–2026
Los Azules	-31.2300	-70.5360	3,408	Río Limari	DGA	Data available only during summer 2025–2026
Nido de Cóndores	-32.6400	-70.0300	5,563	Mendoza	IANIGLA	Poor data quality
Plaza de Mulas	-32.6539	-70.0651	4,320	Mendoza	IANIGLA	Poor data quality between 2018 to 2025
Morenas Coloradas	-32.9601	-69.3700	3,442	Río Mendoza	IANIGLA	Poor data quality
G. Tupungatito Alto	-33.3939	-69.8125	5,500	Río Maipo	DGA	Poor data quality and noisy measurements from 2021 to 2024
Glaciar San Francisco	-33.8040	-70.0710	2,238	Río Maipo	DGA	Poor data quality from 2012 to 2026
Volcán Azufre	-35.3111	-70.5842	3,154	Río Mataquito	DGA	Constant values between 2022–2023; poor data quality
Sierra Velluda	-37.4725	-71.4358	2,702	Río Biobio	DGA	Poor data quality between 2022 and 2025
Cauñicu	-37.7130	-71.4840	621	Río Biobio	DGA	Poor data quality; anomalous peaks during periods without snowfall
Vn. Puyehue	-40.5930	-72.1140	2,120	Río Bueno	DGA	Data since 2026
Monte Tronador	-41.0760	-71.8770	430	Río Petrohue	DGA	No reference height available, but good data series from 2019 to 2025
Vn. Michimahuida Sur	-42.8520	-72.4420	820	Río Yelcho	DGA	Data since 2026
Vc. Yanteles	-43.4464	-72.7914	1,326	Río Corcovado	DGA	Poor data quality during five months in 2024
Teniente Vidal	-45.5970	-72.1140	308	Río Aysen	DGA	Date shift from 2022 to 2025
G. Calluqueo Alto	-47.6000	-72.3990	1,858	Río Baker	DGA	Available data just some months in 2025
Glaciar Lucia	-48.3510	-73.3010	100	Río Pascua	DGA	No data available in 2025
Estero Pantoja	-49.0200	-73.0261	748	Río Pascua	DGA	No data available in 2025
Glaciar Chico	-49.1560	-73.1390	1,611	Río Pascua	DGA	Poor data quality; continuous data between 2022 and 2025
Fiordo Stage	-49.7197	-74.7253	52	Isla Wellington	DGA	Poor data quality from 2023 to 2025
Torre Paine	-51.1750	-72.9540	25	Río Serrano	DGA	Poor data quality from 2023 to 2025
Estación Dorotea	-51.6040	-72.3340	470	Río Hollemberg	DGA	Poor data quality from 2021 to 2025; no ground reference height, but potentially recoverable
Casas Viejas	-51.7000	-72.3260	230	Río Hollemberg	DGA	Poor data quality from 2021 to 2025; no ground reference height
C. Vidal	-52.2410	-72.2030	1,016	Vertiente del Atlántico	DGA	Data since 2026
Villa Tehuelche	-52.4280	-71.4160	190	Rio Penitente	DGA	Poor data quality during several months in 2025
Gran Campo Nevado	-52.8320	-73.2430	166	Costeras e Islas entre R Hollemberg, Golfo Alte. Laguna Blanca	DGA	Data since 2026
Cerro Mirador	-53.1460	-71.0040	580	Costeras e Islas Orientales de la P Brunswick	DGA	Poor data quality from 2022 to 2025; no ground reference height, but potentially recoverable
Pampa Huanaco	-54.0510	-68.8030	150	Río Grande	DGA	No data available for seven months in 2025

https://doi.org/10.5194/essd-2026-324
Preprint. Discussion started: 12 May 2026

Lago deseado	-54.3410	-68.8260	170	Río Grande	DGA	Available data just some months in 2025
Robalo Alto	-54.9780	-67.6740	360	Islas Navarino y Gable	DGA	Available data just some months in 2025

Table A3. Precipitation–year types by river basin identified from percentiles of total precipitation: dry (P0–30), normal (P30–70), and wet (P70–100), based on available data for 2013–2024.

Year	Elqui	Maipo	Maule-Itata
2013	Normal	-	Normal
2014	Dry	Normal	Normal
2015	Wet	Normal	Normal
2016	Wet	Wet	Dry
2017	Normal	Normal	Normal
2018	Normal	Normal	Normal
2019	Dry	Dry	Dry
2020	Dry	Dry	Dry
2021	Dry	Dry	Dry
2022	Wet	Normal	Normal
2023	Dry	Wet	Wet
2024	Wet	Wet	Normal

789

Table A4. Potential and effective total days by station with snow depth data

Station name	Latitude (°)	Raw data				Clean data			
		year start	year end	Potential n° days with data	Effective n° days with data (%)	year start	year end	Potential n° days with data	Effective n° days with data (%)
Vn. Auncanquilcha	-21.2	2021-12-01	2024-12-31	1,127	1,085 (96%)	2021-12-01	2024-12-31	1,127	1,062 (94%)
Cerro Chajnantor	-23.0	2022-03-01	2024-12-31	1,037	733 (71%)	2022-03-01	2024-12-31	1,037	622 (60%)
Vn. Ojos del Salado A.	-27.1	2023-01-03	2024-12-31	729	518 (71%)	2023-01-03	2024-12-31	729	481 (66%)
Vn. Ojos del Salado T.	-27.1	2023-01-03	2024-12-31	729	666 (91%)	2023-01-03	2024-12-31	729	592 (81%)
Glaciar Maranceles	-28.5	2022-04-19	2024-12-31	988	988 (100%)	2022-04-19	2024-12-31	988	975 (99%)
G. Tapado Corrales	-30.2	2020-02-27	2024-12-31	1,770	1,769 (100%)	2020-02-27	2024-12-31	1,770	1,742 (98%)
Tapado (TPF)	-30.2	2018-03-21	2023-10-25	2,045	1,853 (91%)	2018-03-21	2023-10-25	2,045	1,844 (90%)
Los Corrales	-30.2	2022-02-16	2023-07-25	525	343 (65%)	2022-02-16	2023-01-30	349	336 (96%)
Capayan	-30.2	2016-12-20	2024-12-31	2,934	2,933 (100%)	2016-12-20	2024-12-31	2,934	2,892 (99%)
La Laguna	-30.2	2014-06-22	2024-12-31	3,846	2,667 (69%)	2015-06-01	2024-12-31	3,502	2,579 (74%)
Llano de Las Liebres	-30.3	2017-05-16	2024-12-31	2,787	1,295 (46%)	2017-05-16	2021-07-31	1,538	1,098 (71%)
Cerro Olivares	-30.3	2020-12-23	2024-12-31	1,470	1,439 (98%)	2020-12-23	2024-12-31	1,470	735 (50%)
El Jote	-30.4	2019-04-02	2024-12-31	2,101	2,098 (100%)	2019-04-02	2024-12-31	2,101	2,057 (98%)
Quebrada Larga Cota	-30.7	2015-02-20	2024-12-31	3,603	3,428 (95%)	2015-03-07	2024-12-31	3,588	3,373 (94%)
Cerro Vega Negra	-30.9	2015-03-06	2024-10-30	3,527	2,940 (83%)	2016-01-01	2024-10-30	3,226	1,536 (48%)
Tascadero	-31.3	2020-02-19	2024-12-31	1,778	1,299 (73%)	2020-02-19	2024-12-31	1,778	1,282 (72%)
Casa del Canto	-31.4	2019-03-14	2024-12-31	2,120	2,120 (100%)	2019-03-14	2024-12-31	2,120	2,093 (99%)
El Soldado	-32.0	2015-06-08	2024-12-31	3,495	3,319 (95%)	2015-06-08	2024-12-31	3,495	3,099 (89%)
Nacimiento Sobrante	-32.2	2017-01-01	2024-12-31	2,922	2,831 (97%)	2017-01-01	2024-12-31	2,922	2,638 (90%)
Las Cuevas	-32.8	2018-01-03	2024-12-31	2,555	2,553 (100%)	2018-01-03	2024-12-31	2,555	2,543 (100%)

https://doi.org/10.5194/essd-2026-324
Preprint. Discussion started: 12 May 2026

Open Access Earth System Science Data Discussions

Portillo	-32.8	2013-04-24	2024-12-31	4,270	4,258 (100%)	2013-04-24	2024-12-31	4,270	3,748 (88%)
Glaciar León Negro	-33.0	2020-06-10	2024-12-31	1,666	1,392 (84%)	2020-06-10	2024-12-31	1,666	846 (51%)
Glaciar Juncal Sur	-33.1	2019-01-18	2024-12-31	2,175	2,175 (100%)	2019-01-18	2024-12-31	2,175	2,115 (97%)
G. Olivares Gamma	-33.2	2014-05-18	2024-12-31	3,881	3,881 (100%)	2014-05-18	2024-12-31	3,881	3,597 (93%)
Glaciar Olivares Alfa	-33.2	2019-03-26	2024-12-31	2,108	2,008 (95%)	2019-03-26	2024-12-31	2,108	1,954 (93%)
Valle Olivares	-33.2	2014-05-19	2024-12-31	3,880	3,557 (92%)	2015-01-02	2024-12-31	3,652	2,794 (77%)
Yerba Loca Alto	-33.2	2017-10-10	2019-11-22	774	177 (23%)	2017-10-10	2019-11-22	774	176 (23%)
Yerba Loca Medio	-33.3	2016-09-02	2017-10-19	413	364 (88%)	2017-01-01	2017-10-19	292	254 (87%)
Molina en Cepo	-33.3	2017-04-04	2019-11-22	963	118 (12%)	2017-04-04	2017-06-01	59	59 (100%)
Piuquenes10	-33.3	2018-03-11	2020-01-20	681	639 (94%)	2018-05-21	2020-01-20	610	544 (89%)
Piuquenes7	-33.3	2018-03-11	2020-04-24	776	715 (92%)	2018-03-11	2020-04-24	776	702 (90%)
Piuquenes6	-33.3	2018-03-10	2021-12-06	1,368	820 (60%)	2018-03-10	2019-12-31	662	653 (99%)
Piuquenes14	-33.3	2018-03-11	2024-01-09	2,131	2,113 (99%)	2018-05-11	2024-01-09	2,070	1,558 (75%)
La Parva	-33.3	2021-07-20	2024-12-31	1,261	1,261 (100%)	2021-07-20	2024-12-30	1,260	1,236 (98%)
Farellones	-33.4	2023-11-07	2024-12-31	421	420 (100%)	2023-11-07	2024-12-31	421	416 (99%)
Molina Medio	-33.4	2017-04-04	2017-06-01	59	59 (100%)	2017-04-04	2017-06-01	59	58 (98%)
G. Tupungatito Bajo	-33.4	2020-09-24	2024-12-31	1,560	1,560 (100%)	2020-09-24	2024-12-31	1,560	1,342 (86%)
P. G. Echaurren Norte	-33.6	2023-06-07	2024-12-31	574	563 (98%)	2023-06-07	2024-12-31	574	464 (81%)
Valle Echaurren Norte	-33.6	2022-01-12	2024-11-14	1,038	1,028 (99%)	2023-01-01	2024-11-14	684	676 (99%)
Termas Del Plomo	-33.6	2016-01-12	2024-07-04	3,097	2,578 (83%)	2017-03-06	2022-12-31	2,127	1,792 (84%)
Portillo Argentino	-33.6	2020-01-10	2023-04-01	1,178	1,178 (100%)	2020-01-10	2022-12-31	1,087	1,074 (99%)
Laguna Negra	-33.7	2013-04-10	2024-12-31	4,284	3,896 (91%)	2013-04-10	2024-12-31	4,284	3,844 (90%)
Las Melosas	-33.9	2017-01-01	2024-12-31	2,922	2,551 (87%)	2017-01-01	2024-12-31	2,922	2,509 (86%)
Las Hualtatas	-34.1	2021-05-20	2024-12-31	1,322	1,322 (100%)	2021-05-20	2024-12-31	1,322	1,311 (99%)
Codelco Cerro Teniente	-34.2	2024-05-31	2024-12-31	215	215 (100%)	2024-05-31	2024-12-31	215	210 (98%)
Laguna El Yeso	-34.4	2013-04-11	2024-12-31	4,283	2,750 (64%)	2016-01-01	2024-12-31	3,288	1,978 (60%)
Laguna Los Cristales	-34.6	2013-03-09	2024-12-31	4,316	2,724 (63%)	2013-03-09	2018-08-31	2,002	1,282 (64%)
Glaciar Cortaderal	-34.7	2018-05-31	2024-10-13	2,328	2,163 (93%)	2018-05-31	2023-08-31	1,919	1,829 (95%)
G. Universidad	-34.7	2011-06-06	2024-12-31	4,958	2,461 (50%)	2022-05-17	2024-12-31	960	707 (74%)
Cerro Los Guzmanes	-34.9	2024-04-19	2024-12-31	257	253 (98%)	2024-04-19	2024-12-31	257	249 (97%)
Termas Del Flaco	-34.9	2013-04-09	2024-12-31	4,285	3,855 (90%)	2013-04-09	2024-12-31	4,285	3,410 (80%)
Paso Vergara	-35.2	2016-02-18	2024-12-31	3,240	2,910 (90%)	2016-02-18	2024-12-31	3,240	2,145 (66%)
Toqui Lautaro	-35.3	2016-12-06	2024-10-23	2,879	2,560 (89%)	2017-01-01	2024-10-23	2,853	2,529 (89%)
Lo Aguirre	-36.0	2010-06-11	2024-12-31	5,318	5,011 (94%)	2010-06-11	2024-12-31	5,318	3,885 (73%)
Nueva Lo Aguirre	-36.0	2021-06-23	2024-12-31	1,288	1,288 (100%)	2021-06-23	2024-12-31	1,288	1,285 (100%)
Los Condores	-36.0	2014-11-01	2024-12-31	3,714	3,360 (90%)	2015-01-02	2024-12-31	3,652	2,538 (70%)
Nevado Longaví	-36.2	2011-03-01	2024-12-31	5,055	3,911 (77%)	2011-03-01	2024-12-31	5,055	2,934 (58%)
Nevado Chillán	-36.8	2022-05-02	2024-12-31	975	975 (100%)	2022-05-02	2024-12-30	974	491 (50%)
Vn. Chillán	-36.9	2015-03-20	2024-12-31	3,575	3,390 (95%)	2016-03-04	2024-12-31	3,225	3,106 (96%)
Node3	-36.9	2015-01-01	2017-10-12	1,016	1,016 (100%)	2015-01-01	2017-10-12	1,016	1,015 (100%)
Node2	-36.9	2015-01-01	2017-10-12	1,016	1,016 (100%)	2015-01-01	2017-09-05	979	977 (100%)
Node1	-36.9	2015-01-01	2017-10-12	1,016	1,016 (100%)	2015-01-01	2017-10-12	1,016	1,014 (100%)
Node4	-36.9	2015-01-01	2017-10-12	1,016	1,016 (100%)	2015-01-01	2017-08-07	950	948 (100%)
Alto Mallines	-37.2	2015-12-16	2024-12-31	3,304	3,221 (97%)	2016-01-02	2024-12-31	3,287	3,191 (97%)
Los Corralitos	-37.6	2023-03-17	2024-12-31	656	420 (64%)	2023-03-17	2024-12-31	656	419 (64%)
Chenqueco	-38.1	2023-05-31	2024-12-31	581	562 (97%)	2024-01-02	2024-12-31	365	354 (97%)
Liucura	-38.6	2021-11-23	2024-12-31	1,135	1,129 (99%)	2022-01-02	2022-12-31	364	357 (98%)
Vn. Villarrica	-39.4	2021-12-13	2023-11-10	698	478 (68%)	2021-12-13	2023-11-10	698	385 (55%)
Vn.Mocho Choshuenco	-40.0	2019-01-14	2024-12-31	2,179	1,683 (77%)	2024-04-25	2024-12-31	251	207 (82%)
Cardenal Samore	-40.7	2023-04-14	2024-12-31	628	598 (95%)	2023-04-14	2024-12-31	628	592 (94%)
Cuesta Moraga	-43.3	2024-04-26	2024-12-31	250	248 (99%)	2024-04-26	2024-12-31	250	247 (99%)
Cerro Divisadero	-45.6	2023-06-08	2024-12-31	573	481 (84%)	2023-06-08	2024-12-31	573	467 (82%)
Cerro Divisadero Fraile	-45.6	2019-12-31	2024-12-31	1,828	1,743 (95%)	2019-12-31	2024-12-31	1,828	1,056 (58%)

https://doi.org/10.5194/essd-2026-324
Preprint. Discussion started: 12 May 2026

Portezuelo Ibañez	-46.1	2022-07-07	2024-12-31	909	909 (100%)	2022-07-07	2024-12-31	909	906 (100%)
Glaciar San Rafael	-46.7	2015-09-01	2024-12-31	3,410	2,567 (75%)	2021-03-13	2024-12-31	1,390	1,149 (83%)
Steffen	-47.6	2019-12-19	2024-12-31	1,840	1,799 (98%)	2022-01-01	2022-10-09	282	240 (85%)
Epulef	-49.1	2016-01-31	2024-11-05	3,202	1,891 (59%)	2016-01-31	2023-12-31	2,892	1,573 (54%)
Aonikenk	-49.3	2014-03-30	2024-11-10	3,879	3,092 (80%)	2014-03-30	2024-11-10	3,879	3,072 (79%)
Chalten	-49.3	2021-12-09	2024-12-31	1,119	1,089 (97%)	2022-01-01	2024-12-31	1,096	1,053 (96%)
Pliegue Tumbado	-49.4	2020-03-27	2023-04-04	1,104	1,062 (96%)	2020-03-27	2022-12-31	1,010	954 (94%)
Glaciar Snoring	-53.7	2023-08-28	2024-10-14	414	414 (100%)	2024-01-01	2024-10-14	288	285 (99%)

790

Table A5. Summary of raw data reduction of successive quality–control filters for PCI construction.

Station	Total days with SD, Pr and AT simultaneous variables	Season filter (May to October)	Snow accumulation filter (ΔSD > 10 mm)	Precipitation filter (Pr > 1 mm)
Glaciar Tapado Corrales	1,085	546	34	33
Cerro Olivares	705	420	24	21
Glaciar Olivares Alfa	1,992	1,008	114	99
Glaciar Juncal Sur	2,112	1,082	162	151
Glaciar Olivares Gamma	2,095	1,100	68	59
Las Melosas	1,015	548	95	82
Termas Del Plomo	2,245	1,065	182	110

791

Table A6. Summary of clean data reduction of successive quality–control filters for PCI construction.

Station	Total days with SD, Pr and AT simultaneous variables	Season filter (May to October)	Snow accumulation filter (ΔSD > 10 mm)	Precipitation filter (Pr > 1 mm)	AT_{rain}
Glaciar Tapado Corrales	1,066	538	29	28	-2.2
Cerro Olivares	363	182	12	10	2.2
Glaciar Olivares Alfa	1,907	965	78	72	-3.8
Glaciar Juncal Sur	2,063	1,041	113	110	-3.7
Glaciar Olivarea Gamma	1,839	1,050	156	107	-0.9
Las Melosas	983	543	91	79	-1.5
Termas Del Plomo	1,469	710	77	59	3.8

792